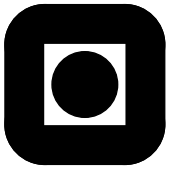
Norges teknisk-naturvitenskapelige universitet - NTNU
Fakultet for naturvitenskap og teknologi
Institutt for fysikk



HOVEDOPPGAVE FOR

STUD. TECHN. JACOB LINDER

Oppgaven gitt: 20.01.2005
Besvarelsen levert: 13.06.2005

FAGOMRÅDE: TEORETISK FYSIKK

Norsk tittel: *"Bruk av koherente vekselvirkninger for å påvirke nøytrinoenes oscillasjonsmønster."*

Engelsk tittel: *"Use of coherent interactions to influence the neutrino oscillation pattern."*

Hovedoppgaven er utført ved Institutt for fysikk, Fakultet for naturvitenskap og teknologi, under veiledning av professor Kåre Olaussen.

Trondheim, 13. juni 2005,

Kåre Olaussen
ansvarlig faglærer
professor ved Institutt for fysikk

Abstract

In this thesis, we explore the possibility to significantely alter the neutrino oscillation probability in matter using realistic detector dimensions. Especially, the implications of a single and multiple non-adiabatic density shifts in the trajectory of a neutrino beam are investigated. As it turns out, there exists a set of resonance parameters in the case of multiple density shifts that gives a full flavor conversion for both neutrinos and antineutrinos, regardless of neutrino source. Although this is an analytical fact, it is not a plausible scenario when restricted to realistic detector densities and lengths. The obtainable results are presented for relevant neutrino species. To make this thesis self-contained, electro-weak theory is briefly reviewed together with the fundamentals of neutrino oscillations and interactions with matter.

Acknowledgments

I would like to thank my excellent supervisor Kåre Olaussen at the Department of Physics, NTNU, for invaluable guidance during the course of this Masters thesis. His insight into the field of theoretical particle physics is most impressive. I also want to thank him for patience and help with my publications, and for simply being good company.

It would be cruel of me not to mention my fellow students Sebastian Ng and Jon Mattis Børven at the Department of Physics, NTNU, and Marius Thaule at the Department of Mathematics, NTNU. They have been a constant source of inspiration and I value their friendship very high.

I am in great debt to Jenny Caroline Wüsthoff, who always has encouraged me to pursue my dreams. Her endless patience and love has been a support I could not have made do without.

Finally, I want to express the acknowledgement of my heart in the words of David, Psalm 23:1-6.

Contents

1 Introduction **1**

2 Standard electro-weak field theory **3**
2.1 Lagrangian and gauge-particles 3
2.2 Neutrino interactions in electro-weak theory 4
2.3 Feynman rules 7

3 Neutrino oscillations **9**
3.1 Fundamental theory 9
3.2 Representation 11

4 Neutrino interactions with matter **13**
4.1 Neutrino cross sections 14
4.2 Matter potentials 20
4.3 MSW-effect for constant electron density 27

5 Exploiting step-wise density shifts **31**
5.1 Single unit-step density profile 31
5.2 Neutrino propagators 36
5.3 Multiple step-wise density profiles 37

6 Detector dimensions and coherence effects **41**
6.1 Statistical analysis 41
6.2 Neutrino coherence 43
6.3 Restrictions on mixing parameters 50

7 Concluding remarks **53**

Bibliography **56**

Chapter 1

Introduction

The neutrino is a leptonic particle which possesses an almost neglible mass of $\mathcal{O}$(eV) (see Sec. 2.2). Since it has no charge, the only experimentally verified interactions are via the weak force. These properties makes the neutrino quite elusive and difficult to observe in detection experiments.

Neutrinos (or $\overline{\nu}$'s to be more specific) were first detected in the famous experiment of Reines and Cowan in the late 50's (see Ref. [1]). They exploited the fact that neutron decay taking place in a nuclear reactor would produce antineutrinos through $n \rightarrow p + e^- + \overline{\nu}_e$. This offered the possibility to look for the signature $\overline{\nu}_e + {}^{37}\mathrm{Cl} \rightarrow e^+ + {}^{37}\mathrm{Ar}$ in a detection setup close to the reactor. The detector itself consisted of $\sim$ 400 l of water mixed with cadmium chloride, in addition to two large scintillation detectors which would serve as photon registrators. When the positron was created, it would almost instantly be annihilated together with an electron from the water, emitting two 0.511 MeV photons in the process. The scintillator detectors would detect these photons and evidence would be at hand for the neutrino-induced reaction.A production of ^{37}Ar was indeed observed, which earned Reines and Cowan the Nobel prize in 1995 for the detection of antineutrinos.

A decade after this discovery, the Homestake neutrino detection site (see Ref. [2]) was designed with the objective to catch neutrinos originating from the sun, specifically from the processes ${}^7\mathrm{Be} + e^- \rightarrow {}^7\mathrm{Li} + \nu_e$ and ${}^8\mathrm{B} \rightarrow {}^8\mathrm{Be} + e^+ + \nu_e$. The Homestake experiment ran consecutively from 1970 - 1992, capturing neutrinos through the inverse β-decay reaction ${}^{37}\mathrm{Cl} + \nu_e \rightarrow {}^{37}\mathrm{Ar} + e^-$. Although the neutrinos certainly turned up in the detector, they did so in a much smaller number than expected from the predictions of the standard solar model (SSM) of the time being. The final results, subtracting estimated background levels, yielded an average of 0.437 ± 0.042 produced ^{37}Ar atoms per day, a number roughly one third of what the SSM predicted. This number was also in reasonable agreement with the observations at the Kamiokande detector (see Ref. [3]) during the period 1987-1990, when both detectors were measuring the solar neutrino flux.

The missing neutrinos were truly a puzzle. However, an interesting concept called *neutrino oscillations* had been proposed by the russian physicist Bruno Pontecorvo in 1958 (see Ref. [4]), not long after the the antineutrino detection experiment of Reines and Cowan. In short, the theory states that the physical neutrino ν_l produced in weak interactions, which comes

in three flavors $l = e, \mu\, \tau$, really is a superposition of so-called mass eigenstates denoted by ν_i, $i = 1, 2, 3$. With each mass eigenstate having a mass m_i, the resulting flavor neutrinos ν_l obtain a time-dependent phase. A quantitative analysis of this scenario gives a well-defined probability to measure a different flavor $\nu_{l'}$ at a given time after the creation of the ν_l (see Sec. 3.1). This will be referred to as the *oscillation probability*.

Introducing neutrino oscillations would explain the solar neutrino deficit. If a ν_e was produced in the sun and during its travel to Earth changed its identity to a ν_μ, it would not be registered by a detector expecting to find an electron-neutrino. The theory of neutrino oscillations has evolved significantly over the years (see *e.g.* Refs. [5, 6]), allowing us to have a pretty clear understanding of neutrino behaviour today. Results from major neutrino detection sites such as SNO and KamLAND (see *e.g.* Refs. [7, 8]) all point in the direction of oscillations being a real phenomena, giving the theory status as the accepted explanation to the missing solar neutrino flux.

The objective of this thesis is to study coherent neutrino interactions with matter, and if it is possible to exploit these matter-effects in terms of significantely altering the oscillation probability. If this is possible, one would obtain additional experimental constraints on the neutrino masses and the magnitude of the mixing between the flavors. These *mixing parameters* are denoted $\{\Delta m^2, \theta\}$, where Δm^2 is the square mass difference between two neutrino mass eigenstates, and θ is the mixing angle that couples flavor- with mass eigenstates. Neutrinos are available from several different sources, ranging from "natural" sources such as the sun, atmosphere or supernovae, to "man-made" sources such as accelerator and reactor neutrinos. Each type of neutrinos carry its own specific fingerprint in terms of for instance kinetic energy E and distance source-detector L_0, often referred to as baseline length. Using the framework of quantum field theory and electro-weak interactions in conjunction with fundamental theory for neutrino oscillations makes it possible to study how the oscillation probability can be manipulated.

This thesis is organized as follows. In chapter 2, neutrino interactions in standard electroweak theory is treated. Chapter 3 deals with fundamental oscillation theory, while neutrino interactions with matter are discussed in chapter 4. The special case of non-adiabatic transitions from vacuum to a medium is given attention in chapter 5. Chapter 6 follows up with a discussion concerning neutrino coherence, in addition to an analysis of the required dimensions for a neutrino detection setup meant to exploit the effect of these non-adiabatic density shifts. Finally, a conclusion is given in chapter 7.

The reader is assumed to have good knowledge of quantum mechanics and some knowledge of field theory. We shall use bold-face notation for three-vectors, *e.g.* $\mathbf{p}$, and italic notation for four-vectors, *e.g.* p. Unless specifically stated otherwise, we will work in natural units $\hbar = c = 1$. Also, we apply Minkowsky metric defined as $\eta^{\mu\nu} = \mathrm{diag}(1, -1, -1, -1)$, and $x^\mu = (t, \mathbf{x})$.

Chapter 2

Standard electro-weak field theory

The standard electro-weak theory is the unification of electromagnetic and weak interactions, and is in agreement with a vast majority of experiments conducted (see *e.g.* Ref. [9]). However, neutrino oscillations have required some revision of the theory since neutrino masses no longer can be assumed to be zero, although they certainly have upper limits as shown in Tab. 2.2. Also, the predicted Higgs boson remains undetected.

This chapter is not meant as an elaborate introduction to the large topic of the electro-weak theory. The intention is to say something about neutrino interactions and techniques used to evaluate particle reactions, which we shall find useful in later sections. We shall mainly stick with the notation of Mandl & Shaw [10].

2.1 Lagrangian and gauge-particles

In the unitary gauge, the Lagrangian density of the standard electro-weak theory is $\mathcal{L} = \mathcal{L}_0 + \mathcal{L}_\mathrm{I}$, where

$$\mathcal{L}_0 = \bar{l}(i\partial\!\!\!/ - m_l)l + \overline{\nu}_l(i\partial\!\!\!/ - m_{\nu_l})\nu_l - \frac{1}{4}A_{\mu\nu}A^{\mu\nu} \tag{2.1}$$

$$- \frac{1}{2}W^\dagger_{\mu\nu}W^{\mu\nu} + m_W^2 W^\dagger_\mu W^\mu - \frac{1}{4}Z_{\mu\nu}Z^{\mu\nu} + \frac{1}{2}m_Z^2 Z_\mu Z^\mu + \frac{1}{2}(\partial^\mu\sigma)(\partial_\mu\sigma) - \frac{1}{2}m_H^2\sigma^2 \tag{2.2}$$

and $\mathcal{L}_\mathrm{I}$ consists of several interaction terms $\mathcal{L}_\mathrm{I}^{(1)} + \mathcal{L}_\mathrm{I}^{(2)} + ...$ responsible for coupling the separate fields. In Eq. (2.1), we have defined $\partial\!\!\!/ \equiv \gamma^\mu\partial_\mu \equiv \gamma^\mu(\partial/\partial x^\mu)$, where γ^μ are the Dirac gamma-matrices (see for instance Mandl & Shaw [10] Appendix A). Also, the abbrevation $X_{\mu\nu} \equiv \partial_\nu X_\mu - \partial_\mu X_\nu$, $X \in \{A, W, Z\}$ has been introduced.

Now, the l- and ν_l-fields describe leptons in the model, while A_μ corresponds to the free electromagnetic field. The $W^\pm$ and Z bosons are described by the W and Z fields, respectively. The terms involving σ constitute the Lagrangian density for a neutral Klein-Gordon field, precisely what we need for a spin zero Higgs boson. Field masses are represented by m_i, $i \in \{l, \nu_l, W, Z, H\}$. The gauge-particles of this theory are given in Tab. 2.1.

The Higgs boson has not yet been discovered, and the best mass estimate as of today is 117 GeV (see the Particle Data Group [11]), just slightly above the highest available energies

Table 2.1: Gauge-particles in standard electro-weak theory. Numerical values obtained from Ref. [11].

Gauge particle	**Mass (GeV)**
Photon, γ	$< 6.000 \times 10^{-26}$
W-boson, $W^{\pm}$	80.43 ± 0.038
Z-boson, Z	91.19 ± 0.002

in the electron-positron accelerator LEP at CERN, before it had to close down in 2000. It is therefore reasonable to assume that the discovery of the Higgs boson is right around the corner, i.e. when the Large Hadron Collider (LHC) in Switzerland becomes operational in 2007, should the Standard Model be correct in its predictions. As pointed out in Ref. [12], electroweak precision data, such as Z pole asymmetries and the W boson mass, are now precise enough to constrain m_H significantly. At a confidence level of 95%, the theoretical upper limit on the mass of the Higgs boson is 205 GeV. Consider Fig. 2.1 taken from Ref. [12] for the mass probability distribution for the Higgs boson. It is worth to note that the probability distribution is a direct result of *a priori* assumptions concerning the validity of experimental e^+e^- collision data from the CERN LEP Collaboration.

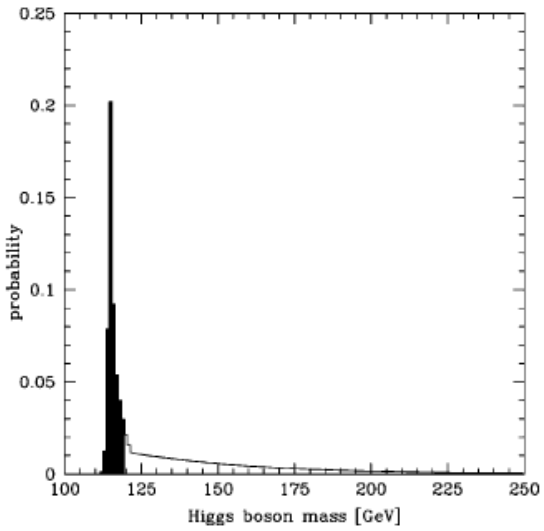


Figure 2.1: Mass probability distribution for the Higgs boson from Ref. [12]. The dark area denotes a total of 50% probability.

2.2 Neutrino interactions in electro-weak theory

Now, all of the interaction terms in $\mathcal{L}_{\mathrm{I}}$ from Sec. 2.1 aren't needed for our purposes. In the following, we shall not consider neutrino interactions with the electromagnetic field $A_\mu(x)$, since the electromagnetic transition moments of the neutrino are too weak for any significant coupling to photons. The upper limit for the neutrino magnetic moment is $\sim 10^{-10}\mu_{\mathrm{B}}$, taken

from the Particle Data Group [11]. When dealing with neutrino interactions, it is sufficient to consider the interaction terms involving W and Z exchange for reactions with ν_l. Higgs exchange will be neglected since it couples very weakly to neutrinos compared to W and Z (see Sec. 4.1.1). The resulting interaction Lagrangian density is then

$$\begin{aligned}\mathcal{L}_{\mathrm{I}} &= \mathcal{L}_{\mathrm{I},W} + \mathcal{L}_{\mathrm{I},Z} \\ &= -\frac{g}{2\sqrt{2}}\big[J^{\mu}_{W}(x)W^{\dagger}_{\mu}(x) + J^{\mu\dagger}_{W}(x)W_{\mu}(x)\big] - \frac{g}{\cos\theta_W}J^{\mu}_{Z}(x)Z_{\mu}(x),\end{aligned} \tag{2.3}$$

where $J^{\mu}_{W}(x)$ and J^{μ}_{Z} are the charged and neutral currents

$$\begin{aligned}J^{\mu}_{W}(x) &= \sum_{l}\bar{l}(x)\gamma^{\mu}(1-\gamma_5)\nu_l(x) \\ J^{\mu}_{Z}(x) &= \frac{1}{4}\sum_{l}\big[\overline{\nu}_l(x)\gamma^{\mu}(1-\gamma_5)\nu_l(x) - \bar{l}(x)\gamma^{\mu}(1-\gamma_5-4\sin^2\theta_W)l(x)\big].\end{aligned} \tag{2.4}$$

In Eq. (2.4), θ_W is the Weinberg angle and g is the weak coupling constant. Now, Eq. (2.3) is valid for all neutrino energies, but we would like to derive an expression for the low-energy limit which often occurs in realistic scattering experiments. More specifically, consider the limit of the external momenta being much smaller than the vector boson masses m_W and m_Z. This means that

$$\begin{aligned}\lim_{m_W^2\gg k^2}\left[\frac{-\mathrm{i}(g_{\mu\nu}-k_\mu k_\nu/m_W^2)}{k^2-m_W^2+\mathrm{i}\epsilon}\right] &= \frac{\mathrm{i}g_{\mu\nu}}{m_W^2} \\ \lim_{m_Z^2\gg k^2}\left[\frac{-\mathrm{i}(g_{\mu\nu}-k_\mu k_\nu/m_Z^2)}{k^2-m_Z^2+\mathrm{i}\epsilon}\right] &= \frac{\mathrm{i}g_{\mu\nu}}{m_Z^2},\end{aligned} \tag{2.5}$$

with $g_{\mu\nu} = \mathrm{diag}(1,\text{-}1,\text{-}1,\text{-}1)$. Making these substitutions corresponds to the interaction transformation in Fig. 2.2, and provides us with the effective interaction Lagrangian density for neutrino interactions (see *e.g.* Ref. [6])

$$\mathcal{L}^{\mathrm{eff}}_{\mathrm{I}} = \mathcal{L}^{\mathrm{eff}}_{\mathrm{I},W} + \mathcal{L}^{\mathrm{eff}}_{\mathrm{I},Z} = -\Big(\frac{g}{2\sqrt{2}}\Big)^2\frac{1}{m_W^2}J^{\mu}_{W}J^{\dagger}_{W\mu} - \Big(\frac{g}{\sqrt{2}\cos\theta_W}\Big)^2\frac{1}{m_Z^2}J^{\mu}_{Z}J^{\dagger}_{Z_\mu}.$$

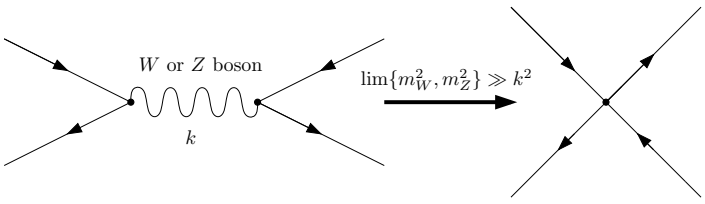


Figure 2.2: Effect of low-energy approximation with dominant m_W and m_Z.

The gauge boson masses are related by $m_W/m_Z = |\cos\theta_W|$. u and d quarks can also be incorporated into this model, merely by adding extra terms to the currents in Eq. (2.4), thus producing

$$
\begin{aligned}
J^{\mu}_{W}(x) &= \sum_{l} \big[\overline{l}(x)\gamma^{\mu}(1-\gamma_5)\nu_l(x)\big] + \overline{d}_{\theta}(x)\gamma^{\mu}(1-\gamma_5)u(x) \\
J^{\mu}_{Z}(x) &= \frac{1}{4}\sum_{l}\big[\overline{\nu}_l(x)\gamma^{\mu}(1-\gamma_5)\nu_l(x) - \overline{l}(x)\gamma^{\mu}(1-\gamma_5-4\sin^2\theta_W)l(x)\big] \\
&\quad + \overline{u}(x)\gamma^{\mu}(1-\gamma_5-\frac{8}{3}\sin^2\theta_W)u(x) - \overline{d}(x)\gamma^{\mu}(1-\gamma_5-\frac{4}{3}\sin^2\theta_W)d(x), \qquad (2.6)
\end{aligned}
$$

where $d_{\theta}(x) = d(x)\cos\theta_C + s(x)\sin\theta_C$. The Cabbibo angle θ_C has been experimentally determined to $\cos\theta_C \approx 0.98$, so we shall exclude the s quark part from now on and set $d_{\theta}(x) = d(x)$. The introduction of quark terms enable us to describe processes such as $\nu_e + n \to p + e$. When adding the quark terms, we have used the general expression for the neutral current found in Quigg [13] p.107-113, namely

$$
J^{\mu}_{Z}(x) = \frac{1}{2}\sum_{i}\overline{\psi}_i(x)\gamma^{\mu}\Big[I^3_i(1-\gamma_5) - 2Q_i\sin^2\theta_W\Big]\psi_i(x), \qquad (2.7)
$$

where $\psi_i = (l, \nu_l, u, d)$, while I^3_i is the belonging particle isospin and Q_i is the particle charge in units of e.

The second quantized expansion for Dirac fields reads

$$
\begin{aligned}
l(x) &= \sum_{s\mathbf{p}}\sqrt{\frac{1}{2VE_{\mathbf{p}}}}\Big[a_s(\mathbf{p})u_s(\mathbf{p})\mathrm{e}^{-\mathrm{i}px} + b^{\dagger}_s(\mathbf{p})v_s(\mathbf{p})\mathrm{e}^{\mathrm{i}px}\Big] \\
\overline{l}(x) &= \sum_{s\mathbf{p}}\sqrt{\frac{1}{2VE_{\mathbf{p}}}}\Big[b_s(\mathbf{p})\overline{v}_s(\mathbf{p})\mathrm{e}^{-\mathrm{i}px} + a^{\dagger}_s(\mathbf{p})\overline{u}_s(\mathbf{p})\mathrm{e}^{\mathrm{i}px}\Big], \qquad (2.8)
\end{aligned}
$$

and similarly for $\nu_l(x), u(x), d(x)$. Here, $E_{\mathbf{p}}$ is the energy of the lepton with momentum $\mathbf{p}$, V is a normalization volume, $\{a_s(\mathbf{p}), a^{\dagger}_s(\mathbf{p})\}$ and $\{b_s(\mathbf{p}), b^{\dagger}_s(\mathbf{p})\}$ are annihilation and creation operators for particles and antiparticles, respectively, while $\{u_s(\mathbf{p}), v_s(\mathbf{p})\}$ are Dirac spinors. Note that $\overline{l}(x) \equiv l^{\dagger}(x)\gamma^0$.

The effective Hamiltonian density is also very useful when doing calculations on for instance scattering reactions. This can be written as $\mathcal{H}^{\mathrm{eff}} = \mathcal{H}^{\mathrm{eff}}_{\mathrm{I},W} + \mathcal{H}^{\mathrm{eff}}_{\mathrm{I},Z}$, where (see *e.g.* Peskin & Schröder [14] chapter 20)

$$
\mathcal{H}^{\mathrm{eff}}_{\mathrm{I},W} = \frac{G_F}{\sqrt{2}}J_{W\mu}J^{\mu\dagger}_{W}, \qquad (2.9)
$$

$$
\mathcal{H}^{\mathrm{eff}}_{\mathrm{I},Z} = \frac{4G_F}{\sqrt{2}}J^{\mu}_{Z}J_{Z\mu}. \qquad (2.10)
$$

We have introduced the Fermi constant, defined as $G_F = \sqrt{2}g^2/8m^2_W$. Eqs. (2.9) and (2.10) will come in handy in chapter 4.

The experimental limits for neutrino masses are given in Tab. 2.2 with data from the Particle Data Group [11]. It is important to realize that these limits are calculated assuming the abscence of mixing, and stem from decay experiments such as ^{3}H- and τ-decay. As pointed out in Ref. [15], the most sensitive experiments with respect to m_{ν_μ} and m_{ν_τ} are 4-6 orders of magnitude less accurate than the best attempts to measure m_{ν_e}. This means that each of the neutrino masses could very well be of order eV or less, which is exactly what is indicated by cosmological constraints introducing the restriction from Ref. [16]

$$\sum_\alpha m_{\nu_\alpha} \leq 1.74 \text{ eV}, \;\; 95\% \text{ C.L.} \tag{2.11}$$

Table 2.2: Neutrino mass limits from particle decays. Numerical values obtained from Ref. [11].

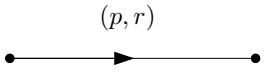
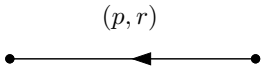
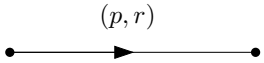
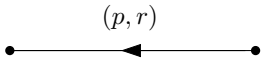
Neutrino type	**Upper mass limit**
ν_e	3 eV
ν_μ	190 keV
ν_τ	18.2 MeV

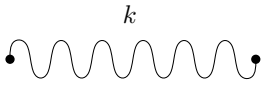
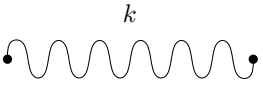
2.3 Feynman rules

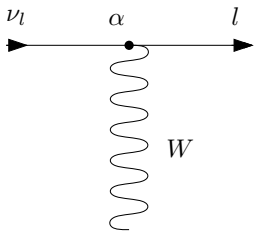
The Feynman diagram is a indispensible tool for analysis of any particle reaction, in order to distuingish between different outcomes and to equip us with an elegant manner of visualizing important physical quantities, such as the cross section. The Feynman amplitude can be read from the diagram with some training and quantifies the process. To set the notation, we give a list of the relevant symbols and algebraic equivalents used in Feynman diagrams describing weak processes for our needs. This is seen in Fig. 2.3. In addition to the already defined symbols, we introduce the axial and vector coupling constants g_A^i and g_V^i, $i \in \{l, \nu_l, u, d\}$. In order to derive these, one needs to start with the condition of local gauge-invariance for the Lagrangian density (see *e.g.* Peskin & Schröder [14] chapter 20). Here, we state the results in Tab. 2.3.

Table 2.3: Relevant weak coupling constants for our needs with $l = \{e, \mu, \tau\}$.

Particle	**Axial coupling** g_A	**Vector coupling** g_V
l	$-1/2$	$2\sin^2\theta_W - 1/2$
ν_l	$1/2$	$1/2$
u	$1/2$	$1/2 - 4\sin^2\theta_W/3$
d	$-1/2$	$2\sin^2\theta_W/3 - 1/2$

EXTERNAL LINES	**SYMBOL**	**FACTOR IN $\mathcal{M}$**
Initial lepton line l^- or ν_l		$u_r(\mathbf{p})$
Initial lepton line l^+ or $\overline{\nu}_l$		$\overline{v}_r(\mathbf{p})$
Final lepton line l^- or ν_l		$\overline{u}_r(\mathbf{p})$
Final lepton line l^+ or $\overline{\nu}_l$		$v_r(\mathbf{p})$

PROPAGATORS	**SYMBOL**	**FACTOR IN $\mathcal{M}$**
Internal W boson		$\frac{\mathrm{i}(-g_{\alpha\beta}+k_\alpha k_\beta/m_W^2)}{k^2-m_W^2+\mathrm{i}\epsilon}$
Internal Z boson		$\frac{\mathrm{i}(-g_{\alpha\beta}+k_\alpha k_\beta/m_Z^2)}{k^2-m_Z^2+\mathrm{i}\epsilon}$

CHARGED CURRENT VERTEX	**SYMBOL**	**FACTOR IN $\mathcal{M}$**
Interaction between leptons $\{l,\nu_l\}$ and W, $l \in \{e,\mu,\tau\}$		$\frac{-\mathrm{i}g}{2\sqrt{2}}\gamma^\alpha(1-\gamma_5)$

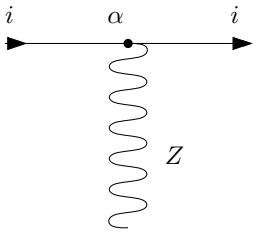
NEUTRAL CURRENT VERTEX	**SYMBOL**	**FACTOR IN $\mathcal{M}$**
Interaction between particle i and Z, $i \in \{l,\nu_l,u,d\}, l \in \{e,\mu,\tau\}$		$\frac{-\mathrm{i}g}{2\cos\theta_W}\gamma^\alpha(g_V^i-g_A^i\gamma_5)$

Figure 2.3: Algebraic expressions for Feynman symbols in standard weak theory, relevant for our needs.

Chapter 3

Neutrino oscillations

In this chapter, we give an introduction to the fundamental theory of neutrino oscillations. Also, the question of Dirac and Majorana neutrinos is briefly reviewed.

3.1 Fundamental theory

Neutrinos are created and absorbed in three different flavors $|\nu_\alpha\rangle$, $\alpha = e, \mu, \tau$, which are linear superpositions of mass eigenstates $|\nu_i\rangle, i = 1, 2, 3$. The mass eigenstates stem from the diagonalization of the Lagrangian density term that couples leptons with the Higgs field, thus providing them with mass. The mixing between these two sets of states is given by

$$|\nu_\alpha(\mathbf{x}, t)\rangle = \sum_{i=1}^{3} U_{\alpha i} |\nu_i(\mathbf{x}, t)\rangle, \tag{3.1}$$

where $|\nu_i(\mathbf{x}, t)\rangle$ is the mass eigenstate with mass m_i, and U is a 3×3 neutrino mixing matrix usually parametrized as in Ref. [6],

$$U = U_{23} U_{13} U_{12} = \begin{bmatrix} 1 & 0 & 0 \\ 0 & c_{23} & s_{23} \\ 0 & -s_{23} & c_{23} \end{bmatrix} \begin{bmatrix} c_{13} & 0 & s_{13} e^{-i\delta_{CP}} \\ 0 & 1 & 0 \\ -s_{13} e^{i\delta_{CP}} & 0 & c_{13} \end{bmatrix} \begin{bmatrix} c_{12} & s_{12} & 0 \\ -s_{12} & c_{12} & 0 \\ 0 & 0 & 1 \end{bmatrix}. \tag{3.2}$$

In Eq. (3.2), $s_{ij} = \sin\theta_{ij}$ and $c_{ij} = \cos\theta_{ij}$, where θ_{ij} are the mixing angles between the neutrino states. δ_{CP} is the CP-violating phase with allowed values $\delta_{CP} \in [0, 2\pi]$. For $\delta_{CP} \in \{0, \pi\}$, we have CP invariance, while the violation is at its largest when $\delta_{CP} \in \{\pi/2, 3\pi/2\}$. For our purposes, δ_{CP} is set to zero. This is commented on in the end of this section. Note that we have intentionally left out diagonal Majorana phases that are of no consequence for oscillation experiments (see Sec. 3.2).

Now, the flavor states are produced and appear in weak interactions, while the mass eigenstates are fit to describe a non-interacting propagating neutrino. Since the flavor states are linear combinations of the mass states, we can invert Eq. (3.1) to obtain $|\nu_i(\mathbf{x}, t)\rangle = \sum_\alpha U^*_{i\alpha} |\nu_\alpha(\mathbf{x}, t)\rangle$. The mass eigenstates are plane waves given as $|\nu_i(\mathbf{x}, t)\rangle \sim e^{i(\mathbf{p}_i \mathbf{x} - E_i t)}$, where $\mathbf{p}_i$ is the momentum and $E_i = \sqrt{\mathbf{p}_i^2 + {m_i}^2}$ is the total energy of mass eigenstate i. The

combination of these relations lead to

$$|\nu_\beta(\mathbf{x},t)\rangle = \sum_{i=1}^{3}\sum_{\alpha} U_{\beta i}U_{i\alpha}^{*}\mathrm{e}^{-\mathrm{i}E_i t}|\nu_\alpha(\mathbf{x},0)\rangle. \tag{3.3}$$

Given that we start off with ν_α, we obtain the probability for an oscillation to have occurred in the ordinary quantum mechanical fashion

$$P_{\nu_\alpha\to\nu_\beta}(t) = |\langle\nu_\alpha(\mathbf{x},0)|\nu_\beta(\mathbf{x},t)\rangle|^2. \tag{3.4}$$

Direct insertion of our quantities yields

$$P_{\nu_\alpha\to\nu_\beta}(t) = \Big|\sum_{i=1}^{3} U_{\beta i}U_{i\alpha}^{*}\mathrm{e}^{-\mathrm{i}E_i t}\Big|^2. \tag{3.5}$$

Here, we have demanded that mass eigenstates satisfy the orthonormality condition

$$\langle\nu_i(\mathbf{x},t)|\nu_j(\mathbf{x},t)\rangle = \delta_{ij}. \tag{3.6}$$

Assuming equal momentum $|\mathbf{p}_i| \equiv E$ for all neutrinos and taking the masses as small compared to this momentum, $E_i = \sqrt{\mathbf{p}_i^2 + {m_i}^2} \simeq E + {m_i}^2/2E$, we arrive at our final result for the three-flavor scenario

$$P_{\nu_\alpha\to\nu_\beta}(t) = \sum_{\substack{i\in 1,2,3\\ j\in 1,2,3}} J_{\alpha\beta ij}\mathrm{e}^{-\mathrm{i}\Delta m_{ij}^2 t/2E} \tag{3.7}$$

with $J_{\alpha\beta ij} = U_{\beta i}U_{i\alpha}^{*}U_{\beta j}^{*}U_{j\alpha}$. Δm_{ij}^2 is the square mass difference and E is the neutrino kinetic energy. Although Eq. (3.7) might look suspicious with respect to being a real quantity, which we humbly must insist on for a probability function, the reader should not be alarmed. $P_{\nu_\alpha\to\nu_\beta}$ is expressed in this compact manner for aesthetic reasons, and it is easily verified that $J_{\alpha\beta ij} = J_{\alpha\beta ji}^{*}$. The exponential terms $\exp(-\mathrm{i}\Delta m_{ij}^2 t/2E)$ also find matching partners in the sum over $\{i,j\}$ to form real cosine and sine terms.

Neutrinos are ultrarelativistic due to their tiny mass, i.e. $E_i \simeq E$, which means that the time-dependent exponential factor is almost exactly identical in either case. It is true that the validity of this argument seems questionable when considering Tab. 2.2. A tau-neutrino mass of $m_{\nu_\tau} \simeq 18$ MeV hardly can be dismissed as "tiny" compared to for instance solar neutrino kinetic energies of $\mathcal{O}(\mathrm{MeV})$. Our justification of treating the neutrino masses as very small is given at the end of Sec. 2.2.

In the two-flavor scenario, the relation between flavor and mass eigenstates is parametrized by a 2×2 mixing matrix U, reading

$$\begin{bmatrix} \nu_e \\ \nu_\mu \end{bmatrix} = \overbrace{\begin{bmatrix} c_\theta & s_\theta \\ -s_\theta & c_\theta \end{bmatrix}}^{U} \begin{bmatrix} \nu_1 \\ \nu_2 \end{bmatrix} \tag{3.8}$$

for the $\{\nu_e,\nu_\mu\}$ case. The exact probability amplitude is calculated in the same way as for three flavors. With $\{\alpha,\beta\}$ designating neutrino flavor and Δm^2 equal to the square mass difference of the two mass eigenstates, it is found that

$$P_{\nu_\alpha\to\nu_\beta}(t) = \overbrace{\sin^2(2\theta)}^{\text{Amplitude term}} \times \overbrace{\sin^2\frac{t\Delta m^2}{4E}}^{\text{Oscillation term}}, \quad (\alpha\neq\beta). \tag{3.9}$$

In the following, we shall name the amplitude term $\mathcal{A}$ and the oscillation term $\mathcal{W}$. The frequently used expression for probability amplitude of two-flavor oscillations in vacuum is obtained by extracting proper numerical constants, leaving us with

$$P_{\nu_\alpha \to \nu_\beta} = \sin^2(2\theta) \times \sin^2 \frac{1.27 L(\text{km}) \Delta m^2(\text{eV}^2)}{E(\text{GeV})}, \ (\alpha \neq \beta). \tag{3.10}$$

The transition from Eq. (3.9) to Eq. (3.10) was mediated by the very good approximation that neutrinos travel with the speed of light, so that $t = L$ in natural units. Neutrino flavor conservation dictates that $P_{\nu_\alpha \to \nu_\alpha} = 1 - P_{\nu_\alpha \to \nu_\beta}$.

In the following, we shall use the notation $\Delta m^2_{\text{SOL}} \equiv \Delta m^2_{12}$, $\theta_{\text{SOL}} \equiv \theta_{12}$, $\Delta m^2_{\text{ATM}} \equiv \Delta m^2_{23}$, $\theta_{\text{ATM}} \equiv \theta_{23}$. The reason is simply that the set of parameters that best describes solar neutrino data from experimental sites such as Super-Kamiokande and SNO involves Δm^2_{12} and θ_{12}, while atmospheric neutrino data from the Kamiokande detector in particular are described by Δm^2_{23} and θ_{23}. Thus, experimental data indicate that the solar and atmospheric neutrino oscillations constitute two decoupled 2-flavor scenarios, i.e. $\theta_{13} \simeq 0$. When comparing to Eq. (3.2), we see that $U_{23} = U_{\text{ATM}}$ and $U_{12} = U_{\text{SOL}}$. The observed solar neutrino oscillations involve $\nu_e \leftrightarrow \nu_\mu$ with a small fraction of $\nu_e \leftrightarrow \nu_\tau$, while atmospheric neutrino oscillations read $\nu_\mu \leftrightarrow \nu_\tau$. Tab. 3.1 from Ref. [17] presents todays best-fit values for neutrino parameters with belonging confidence intervals, assuming normal mass hierarchy $m_3 > m_2 > m_1$.

Table 3.1: Values for neutrino parameters from Ref. [17].

Parameter	Best-fit	Range	Confidence Level
Δm^2_{SOL}	7.1×10^{-5} eV^2	$[6.0, 9.0] \times 10^{-5}$ eV^2	99%
Δm^2_{ATM}	2.5×10^{-3} eV^2	$[1.3, 3.9] \times 10^{-3}$ eV^2	90%
θ_{SOL}	0.59 rad	[0.47, 0.77] rad	99%
θ_{ATM}	0.78 rad	[0.65, 0.78] rad	90%
θ_{13}	n/a	[0.00, 0.16] rad	90%

As is seen in Tab. 3.1, the value of θ_{13} still suffers from a significant uncertainty, although reactor neutrino experiments such as CHOOZ (see *e.g.* Ref. [18]) have been helpful in assigning upper limits to its value. Now, in the beginning of this section we set the CP-violating phase equal to zero. A non-zero value of θ_{13} is actually necessary to enable CP-violation in the lepton-sector of the standard model. Due to the smallness of θ_{13}, we assume that it is safe to set $\delta_{\text{CP}} = 0$.

3.2 Representation

A neutrino state can be described by two different representations. The Dirac representation is based upon the assumption of particles and antiparticles having unequal physical properties. This is the only real alternative for the electron and positron, for instance, since they have opposite electrical charge. On the other hand, a Majorana representation is necessary for spin $\frac{1}{2}$ particles that are identical to their antiparticles, like the $s = 1$ photons are.

This definition is rather crude. A more sophisticated argument is presented in Boehm & Vogel [19] chapter 1, and goes as follows. A massive left-handed neutrino ν^L, i.e. with negative helicity (momentum antiparallel to spin), can always be turned into a right-handed neutrino ν^R by a Lorentz boost to a frame of reference moving faster than the neutrino itself. If we instead operate with CPT on the ν^L, it is turned into a right-handed antineutrino $\overline{\nu}^R$. Similarly, a $\overline{\nu}^L$ is created by operating with CPT on a ν^R. The punchline is that if all of these four states $\{\nu^L, \nu^R, \overline{\nu}^L, \overline{\nu}^R\}$ are distinct, then the neutrino is a Dirac particle. But if the $\nu^L(\nu^R)$ and $\overline{\nu}^L(\overline{\nu}^R)$ states are equal, i.e. the effect of CPT is the same as a Lorentz boost, then the neutrino is a Majorana particle.

The neutrino-case is unfortunately not a clear cut. Most experiments before the new millenium indicated that the best-fit values of Δm^2 for the neutrino and corresponding antineutrino flavors seemed to be equal, i.e. $m^2_{\nu_\alpha} - m^2_{\nu_\beta} = m^2_{\overline{\nu}_\alpha} - m^2_{\overline{\nu}_\beta}$. The so-called LSND anomaly (see Ref. [20]) stirred things up in 1999 when the results demanded an square mass difference of $\Delta m^2 \simeq 1$ eV^2 for $\overline{\nu}_\mu \to \overline{\nu}_e$ oscillations, a number far greater than the best-fit value $\Delta m^2_{\text{SOL}} = 7.1 \times 10^{-5}$ eV^2 for the $\nu_\mu \to \nu_e$ scenario. As a consequence, the neutrino would have to be a Dirac particle since the antineutrino possessed a different mass, in addition to CPT-invariance being violated in the standard model.

Should the LSND results turn out to be valid one of two things will happen. One option is to abandon the theorem of CPT-invariance, but this is a highly unattractive alternative since the CPT-theorem constitutes a cornerstone in relativistic quantum field theory. The second option would be to introduce a fourth, sterile (non-interacting) neutrino flavor to explain the results. But this option is not particularly welcome either ever since the triumph at the Sudbury Neutrino Observatory (SNO) in 2001 (see Ref. [8]). In this experiment, the total detected neutrino flux of active, as opposed to sterile, neutrinos ν_l was consistent with theoretical predictions of the electron-neutrino production in the sun, i.e. $\Phi_e^{\text{Sun}} = \Phi_e^{\text{SNO}} + \Phi_\mu^{\text{SNO}} + \Phi_\tau^{\text{SNO}}$. This result is the strongest evidence yet of three-flavor oscillations occuring, thus pretty much ruling out the existence of a fourth, sterile neutrino flavor.

The MiniBOONE experiment conducted at Fermilab, USA (see *e.g.* Ref. [21]) is specifically designed to check the results of LSND, and will be of great importance in determining whether CPT-violation is actually happening. Neutrino detection experiments cannot in themselves determine whether the neutrino is a Dirac or Majorana particle. However, the neutrinoless double beta decay ${}^Z_A X \to {}^A_{Z+2} X + 2e$ offers the possibility to determine the Dirac-Majorana argument for the neutrino (see *e.g.* Boehm & Vogel [19] chapter 6). In ordinary double beta decay, two antineutrinos are emitted with the electrons. But if the neutrino is its own antiparticle, the neutrinos could annihilate eachother and result in neutrinoless beta decay. Up to this date, there is no compelling evidence in either direction concerning Dirac or Majorana neutrinos.

Chapter 4

Neutrino interactions with matter

The reactions in which neutrinos mainly participate with matter on Earth and the belonging Feynman diagrams are shown in Fig. 4.1.

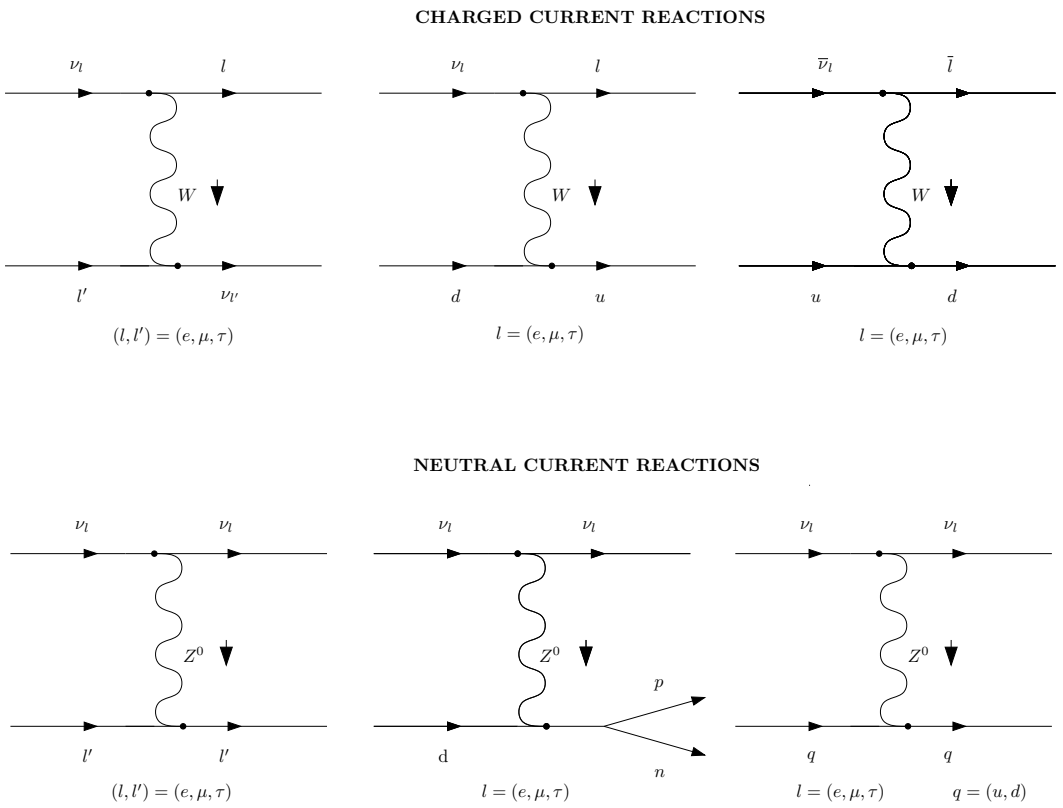


Figure 4.1: Neutrino reactions with matter on Earth types and their corresponding Feynman diagrams.

Note that we have intentionally left out the reactions mediated by the Higgs boson H for reasons that will become apparent in Sec. 4.1.1. The reactions in Fig. 4.1 become important as we leave the vacuum scenario of neutrino oscillations and turn our attention to oscillations in matter. The vacuum oscillation probability is given in Eq. (3.9), but this expression is

modified when the neutrinos travel through matter, due to the so-called MSW-effect (see Ref. [22]), named after the physicists Mikheyev, Smirnov, and Wolfenstein. The MSW-effect favors certain neutrino reactions, dependent on the medium. For instance, since Earth has an excess of electrons compared to muons and tauons, ν_e will acquire a charged current contribution to the reaction $\nu_e + e \to \nu_e + e$. The ν_μ and ν_τ, however, will still only interact with the Z boson. Thus, the balance is shifted in the favor of the electron-neutrinos.

We briefly review relevant neutrino cross sections, before we calculate matter potentials induced by Earth and the resulting MSW-effect.

4.1 Neutrino cross sections

The differential cross section $\mathrm{d}\sigma$ says something about how incoming particles are scattered in space, and the likelihood of the scattering to occur at all. More precisely, since the interpretation of σ is the number of particles scattered into a specific final state per unit time divided on the incident flux, the expression for $\mathrm{d}\sigma$ is

$$\mathrm{d}\sigma = \frac{wV}{v_{\mathrm{rel}}} \times \prod_f \frac{V \mathrm{d}\mathbf{p}'_f}{(2\pi)^3}, \tag{4.1}$$

where w is the transition probability from $|i\rangle$ to $|f\rangle$ per unit time, v_{rel} is the relative velocity between incident and target particles, and $\prod_f \frac{V \mathrm{d}\mathbf{p}'_f}{(2\pi)^3}$ is the number of states with momentum in the interval $(\mathbf{p}'_f, \mathbf{p}'_f + \mathrm{d}\mathbf{p}'_f)$. In the special case of two incoming particles, the differential cross section reads

$$\mathrm{d}\sigma = \frac{1}{4E_1E_2v_{\mathrm{rel}}}(2\pi)^4\delta^{(4)}\Big(\sum_f p'_f - \sum_i p_i\Big)\prod_f \frac{\mathrm{d}\mathbf{p}'_f}{(2\pi)^3 2E'_f}|\mathcal{M}|^2, \tag{4.2}$$

where p_i are the 4-momenta of the incoming particles, p'_f are the 4-momenta of the outgoing particles, and $\mathcal{M}$ is the Feynman amplitude of the process. Calculations are often simplified when considering the process from the Center-of-Mass (CM) system. There, Eq. (4.2) is reduced to

$$\Big(\frac{\mathrm{d}\sigma}{\mathrm{d}\Omega}\Big)_{\mathrm{CM}} = \frac{1}{64\pi^2(E_1+E_2)^2}\frac{|\mathbf{p}'_1|}{|\mathbf{p}_1|}|\mathcal{M}|^2. \tag{4.3}$$

For a detailed derivation of these quantities, consider Mandl & Shaw [10] chapter 7 and 8. Note that we have chosen a slightly different normalization of the Feynman amplitude compared to Ref. [10], excluding a factor $2m$ for each of the interacting particles, where m is the particle mass.

In the following sections, we first give attention to neutral current neutrino-fermion scattering. Next, we generalize to charged current reactions mediated by the W boson.

4.1.1 Neutral current scattering

To begin with, we shall consider $\nu_l f$ $(l \neq f)$ scattering, where l is a lepton and f is a fermion. This process is only mediated by the Z boson, if we disregard the Higgs boson as a gauge particle. The reason for this is the fact that the Feynman amplitude corresponding to the

scattering process mediated by H is of $\mathcal{O}(m_{\nu_l} m_f / m_H^2)$ compared to the Z diagram. Now, the only relevant lowest order Feynman diagram for $\nu_l f$ $(l \neq f)$ scattering is shown in Fig. 4.2. Using our Feynman rules from Sec. 2.3 gives the Feynman amplitude

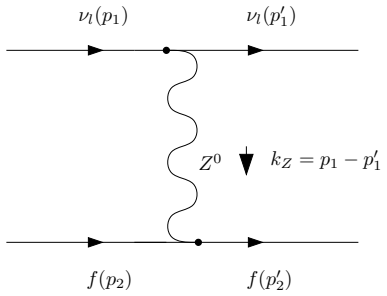


Figure 4.2: Lowest contributing order Feynman diagrams for $\nu_l + f \to \nu_l + f$.

$$\mathcal{M} = \overline{u}_{\nu_l}(1')[-\frac{\mathrm{i}g}{2\cos\theta_W}\gamma^\alpha(g_V^{\nu_l} - g_A^{\nu_l}\gamma_5)]u_{\nu_f}(1)\mathrm{i}\Big(\frac{-g_{\alpha\beta} + k_{Z\alpha}k_{Z\beta}/m_Z^2}{k_Z^2 - m_Z^2 + \mathrm{i}\epsilon}\Big)$$
$$\times\ \overline{u}_f(2')[-\frac{\mathrm{i}g\gamma^\beta}{2\cos\theta_W}(g_V^f - g_A^f\gamma_5)]u_f(2,)$$

Observe that we have shortened down $u_{s_i}(\mathbf{p}_i)$ to $u(i)$, and are using the general coupling constants g_V and g_A for the neutrino and the fermion, although Sec. 2.2 already has revealed these to be equal to $1/2$ for neutrinos. These expressions can be simplified a great deal, when making some considerations. It is reasonable to expect $m_W^2 \gg k_W^2$ when using $m_W = 80.4$ GeV for the intermediate vector boson $W^\pm$. The same inequality goes for $m_Z = 91.2$ GeV and $m_H \geq 112$ GeV. By applying this low-energy limit, we regain the effective propagator from Sec. 2.2, arriving at

$$\mathcal{M} = \frac{-2\mathrm{i}G_F}{\sqrt{2}}\overline{u}_{\nu_l}(1')[\gamma^\alpha(g_V^{\nu_l} - g_A^{\nu_l}\gamma_5)]u_{\nu_l}(1)\overline{u}_f(2')[\gamma_\alpha(g_V^f - g_A^f\gamma_5)]u_f(2). \tag{4.4}$$

We now pursue the absolute square of the Feynman amplitude, $|\mathcal{M}|^2$, which is part of the differential cross section in Eq. (4.3). In a perfect world, the polarization, i.e. spins, of the reacting particles would be known. Unfortunately, this is the exception rather than the rule. If one does not know the initial and final spins of the neutrinos and electrons, this must be compensated for by averaging over the incoming spin states and adding the final states. This normally corresponds to an averaging factor of $1/2$ and summation of spins for each incoming particle.

Neutrinos, however, are special cases. Although they are massive, their mass is so small that it is ordinarily set to zero in the standard model. This means that there is only one helicity state for the neutrino, since it consequently travels with the speed of light and never can be overcome in any Lorentz frame. Neutrinos are therefore not expected to be unpolarized, but retain the left-handed helicity state they were originally created with. Thus, there is only one spin state to consider for the neutrinos. We therefore perform the substitution

$$|\mathcal{M}|^2 \to \frac{1}{2}\sum_{s_i, s_f'} |\mathcal{M}|^2$$

in order to obtain the unpolarized cross-section. By exploiting the fact that $|\mathcal{M}|^2 = \mathcal{M}\mathcal{M}^*$ and $(\gamma^\mu)^\dagger = \gamma^0\gamma^\mu\gamma^0$, the problem is attacked. Inserting Eq. (4.4) gives

$$\frac{1}{2}\sum_{s_i,s_f'}|\mathcal{M}|^2 = \frac{1}{2}\sum_{s_i,s_f'}\left[\frac{-2\mathrm{i}G_F}{\sqrt{2}}\overline{u}_{\nu_l}(1')\gamma^\alpha(g_V^{\nu_l}-g_A^{\nu_l}\gamma_5)u_{\nu_f}(1)\overline{u}_f(2')\gamma_\alpha(g_V^f-g_A^f\gamma_5)u_f(2)\right]$$
$$\times\left[\frac{2\mathrm{i}G_F}{\sqrt{2}}\overline{u}_f(2)\gamma_\beta(g_V^f-g_A^f\gamma_5)u_f(2')\overline{u}_{\nu_l}(1)\gamma^\beta(g_V^{\nu_l}-g_A^{\nu_l}\gamma_5)u_{\nu_l}(1')\right]$$

We stride on by recalling the completeness relations for the Dirac spinors u and v

$$\sum_s u_{l\alpha}(p,s)\overline{u}_{l\beta}(p,s) = (\not{p}+m_l)_{\alpha\beta}, \quad \sum_s v_{l\alpha}(p,s)\overline{v}_{l\beta}(p,s) = (\not{p}-m_l)_{\alpha\beta}.$$

Attaching indices on spinors and matrices provides us with

$$\frac{1}{2}\sum_{s_i,s_f'}|\mathcal{M}|^2 = G_F^2\sum_{s_i,s_f'}\left[\overline{u}_{\nu_l\kappa}(1')\Big[\gamma^\alpha(g_V^{\nu_l}-g_A^{\nu_l}\gamma_5)\Big]_{\kappa\lambda}u_{\nu_l\lambda}(1)\overline{u}_{f\gamma}(2')\Big[\gamma_\alpha(g_V^f-g_A^f\gamma_5)\Big]_{\gamma\delta}u_{f\delta}(2)\right]$$
$$\times\left[\overline{u}_{f\epsilon}(2)\Big[\gamma_\beta(g_V^f-g_A^f\gamma_5)\Big]_{\epsilon\tau}u_{f\tau}(2')\overline{u}_{\nu_l\sigma}(1)\Big[\gamma^\beta(g_V^{\nu_l}-g_A^{\nu_l}\gamma_5)\Big]_{\sigma\rho}u_{\nu_l\rho}(1')\right]$$
$$= G_F^2\mathrm{Tr}\Big\{(\not{p}_1'+m_{\nu_l})\gamma^\alpha(g_V^{\nu_l}-g_A^{\nu_l}\gamma_5)(\not{p}_1+m_{\nu_l})\gamma^\beta(g_V^{\nu_l}-g_A^{\nu_l}\gamma_5)\Big\}$$
$$\times\mathrm{Tr}\Big\{(\not{p}_2'+m_f)\gamma_\alpha(g_V^f-g_A^f\gamma_5)(\not{p}_2+m_f)\gamma_\beta(g_V^f-g_A^f\gamma_5)\Big\}. \tag{4.5}$$

We designate

$$① = \mathrm{Tr}\Big\{(\not{p}_1'+m_{\nu_l})\gamma^\alpha(g_V^{\nu_l}-g_A^{\nu_l}\gamma_5)(\not{p}_1+m_{\nu_l})\gamma^\beta(g_V^{\nu_l}-g_A^{\nu_l}\gamma_5)\Big\}$$
$$② = \mathrm{Tr}\Big\{(\not{p}_2'+m_f)\gamma_\alpha(g_V^f-g_A^f\gamma_5)(\not{p}_2+m_f)\gamma_\beta(g_V^f-g_A^f\gamma_5)\Big\}, \tag{4.6}$$

and consider each of the traces separately. Using the general relations for traces

$$\mathrm{Tr}\{A+B+...\} = \mathrm{Tr}\{A\}+\mathrm{Tr}\{B\}+...$$
$$\mathrm{Tr}\{\gamma^5\} = \mathrm{Tr}\{\gamma^5\gamma^\alpha\} = \mathrm{Tr}\{\gamma^5\gamma^\alpha\gamma^\beta\} = \mathrm{Tr}\{\gamma^5\gamma^\alpha\gamma^\beta\gamma^\gamma\} = 0$$
$$\mathrm{Tr}\{\gamma^5\gamma^\alpha\gamma^\beta\gamma^\gamma\gamma^\delta\} = -4\mathrm{i}\epsilon^{\alpha\beta\gamma\delta}$$
$$\mathrm{Tr}\{\gamma^\alpha\gamma^\beta...\gamma^\rho\gamma^\sigma\} = 0 \text{ if } \gamma^\alpha\gamma^\beta...\gamma^\rho\gamma^\sigma\text{is an odd number of } \gamma\text{-matrices}, \tag{4.7}$$

where $\epsilon^{\alpha\beta\gamma\delta}$ is a completely antisymmetric tensor, we obtain

$$① = 8p_{1\mu}'p_{1\nu}\Big[\mathrm{i}g_V^{\nu_l}g_A^{\nu_l}\epsilon^{\mu\alpha\nu\beta}+\frac{1}{2}[(g_V^{\nu_l})^2+(g_A^{\nu_l})^2](\eta^{\mu\alpha}\eta^{\nu\beta}+\eta^{\mu\beta}\eta^{\nu\alpha}-\eta^{\mu\nu}\eta^{\alpha\beta})\Big]$$
$$② = 8p_2'^\sigma p_2^\rho\Big[\mathrm{i}g_V^f g_A^f\epsilon_{\sigma\alpha\rho\beta}+\frac{1}{2}[(g_V^f)^2+(g_A^f)^2](\eta_{\sigma\beta}\eta_{\rho\alpha}+\eta_{\sigma\alpha}\eta_{\rho\beta}-\eta_{\sigma\rho}\eta_{\alpha\beta})\Big]+4m_f^2(g_V^2-g_A^2)\eta_{\alpha\beta} \tag{4.8}$$

in the limit $m_{\nu_l} \to 0$. From Eq. (4.3) we see that the differential cross-section in the CM system must be

$$\Big(\frac{\mathrm{d}\sigma}{\mathrm{d}\Omega}\Big)_{\mathrm{CM}} = \frac{X}{64\pi^2(E_1+E_2)^2}\frac{|\mathbf{p}_1'|}{|\mathbf{p}_1|}, \tag{4.9}$$

where

$$X = \frac{1}{2}\sum_{s_i,s_f'} |\mathcal{M}|^2 = G_F^2\big[① \times ②\big].$$

The product of the two traces is

$$\begin{aligned} ① \times ② = {} & 128 g_V^f g_A^f g_V^{\nu_l} g_A^{\nu_l}\big[(p_1'p_2')(p_1p_2) - (p_1'p_2)(p_1p_2')\big] \\ & + 32[(g_V^f)^2 + (g_A^f)^2][(g_V^{\nu_l})^2 + (g_A^{\nu_l})^2]\big[(p_1'p_2)(p_1p_2') + (p_1'p_2')(p_1p_2)\big] \\ & - 32m_f^2[(g_V^f)^2 - (g_A^f)^2][(g_V^{\nu_l})^2 + (g_A^{\nu_l})^2](p_1'p_1). \end{aligned} \tag{4.10}$$

Our situation now looks like Fig. 4.3 in the CM frame with 4-momenta

$$\begin{aligned} p_1 &= (E,0,0,E), \\ p_2 &= (\sqrt{E^2+m_f^2},0,0,-E), \\ p_1' &= E(1,\cos\phi\sin\theta,\sin\phi\sin\theta,\cos\theta), \\ p_2' &= (\sqrt{E^2+m_f^2},-E\cos\phi\sin\theta,-E\sin\phi\sin\theta,-E\cos\theta), \end{aligned} \tag{4.11}$$

where $E \equiv E_{\mathrm{CM}}$ is the CM kinetic energy of the neutrino. Since all 4-momenta now are

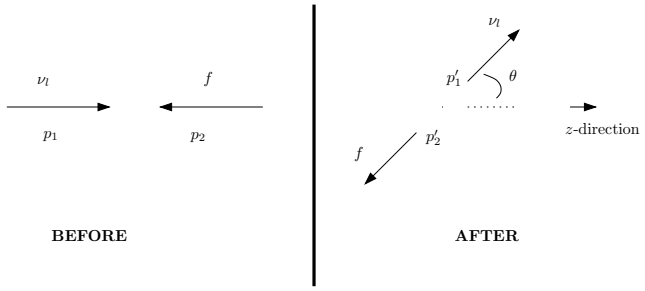


Figure 4.3: $\nu_l f$ $(l \neq f)$ scattering in the CM frame.

known, insertion of Eq. (4.11) into Eq. (4.10) gives

$$\begin{aligned} ① \times ② = {} & 128 g_V^f g_A^f g_V^{\nu_l} g_A^{\nu_l}\big[(E\sqrt{E^2+m_f^2}+E^2)^2 - (E\sqrt{E^2+m_f^2}+E^2\cos\theta)^2\big] \\ & + 32[(g_V^f)^2 + (g_A^f)^2][(g_V^{\nu_l})^2 + (g_A^{\nu_l})^2]\big[(E\sqrt{E^2+m_f^2}+E^2)^2 + (E\sqrt{E^2+m_f^2}+E^2\cos\theta)^2\big] \\ & - 32m_f^2[(g_V^f)^2 - (g_A^f)^2][(g_V^{\nu_l})^2 + (g_A^{\nu_l})^2]E^2(1-\cos\theta). \end{aligned} \tag{4.12}$$

The total cross section for $\nu_l f$ $(l \neq f)$ scattering is now within our grasp, and reads

$$\sigma[\nu_l f\ (l \neq f)] = \frac{G_F^2}{32\pi(E+\sqrt{E^2+m_f^2})^2}\int_0^\pi [① \times ②]\sin\theta\ \mathrm{d}\theta. \tag{4.13}$$

From Eq. (4.12), it is clear that we must evaluate three types of integrals, namely

$$\int_0^\pi \sin\theta \ \mathrm{d}\theta = 2, \ \int_0^\pi \cos\theta \sin\theta \ \mathrm{d}\theta = 0, \ \int_0^\pi \cos^2\theta \sin\theta \ \mathrm{d}\theta = \frac{2}{3}. \tag{4.14}$$

Note that $s = (p_1 + p_2)^2 = (E + \sqrt{E^2 + m_f^2})^2$. At this point, we insert the neutrino coupling constants $g_V^{\nu_l} = g_A^{\nu_l} = 1/2$ and our integrals Eq. (4.14) into Eq. (4.13), which consequently reduces to

$$\sigma[\nu_l f \ (f \neq l)] = \frac{G_F^2 (s - m_f^2)^2}{4\pi s} \Bigg[(g_V^f + g_A^f)^2 + (g_V^f - g_A^f)^2 \Big[\frac{m_f^2}{s} + \frac{(s - m_f^2)^2}{3s^2} \Big] - [(g_V^f)^2 - (g_A^f)^2] \frac{m_f^2}{s} \Bigg]. \tag{4.15}$$

Eq. (4.15) provides us with the total cross section for neutrino-fermion scattering processes mediated by Z. The cross section for antineutrino-fermion scattering $\overline{\nu}_l f (f \neq l)$ is obtained from the following argumentation. In the limit $m_{\nu_l} \to 0, l = e, \mu, \tau$, neutrinos are always left-handed while antineutrinos will be right-handed. Thus, only a parity transformation $\mathcal{P}$ on the neutrino vertex part of the Feynman amplitude Eq. (4.4) is required to obtain $\overline{\nu}_l l' \ (l \neq l')$ scattering. Now, a scalar product of two axial vectors is invariant under a parity transformation, and so is the scalar product of the vector quantities as well. Recall that axial vectors $y^\mu = (y^0, \mathbf{y})$ transform as $y^\mu \overset{\mathcal{P}}{\longmapsto} \widetilde{y}^\mu = (-y^0, \mathbf{y})$ under parity, while vector quantities $z^\mu = (z^0, \mathbf{z})$ transform as $z^\mu \overset{\mathcal{P}}{\longmapsto} \widetilde{z}^\mu = (z^0, -\mathbf{z})$. Thus, it follows that the scalar product of a axial and vector quantity is not invariant under parity transformations, since

$$y^\mu z_\mu \overset{\mathcal{P}}{\longmapsto} \widetilde{y}^\mu \widetilde{z}_\mu = -y^0 z_0 + \mathbf{yz} = -y^\mu z_\mu \tag{4.16}$$

As a consequence, all mixed terms $g_V^{\nu_l} g_A^{\nu_l}$ will change sign. This means that the cross section for antineutrino-fermion scattering is found by making the substitutions

$$\sigma[\overline{\nu}_l f \ (l \neq f)] = \lim_{g_V^{\nu_l} g_A^{\nu_l} \to (-g_V^{\nu_l} g_A^{\nu_l})} \sigma[\nu_l f \ (l \neq f)]. \tag{4.17}$$

For $\overline{\nu}_l \overline{f} \ (l \neq f)$ scattering, $g_V^f g_A^f$ will also change sign, yielding

$$\sigma[\overline{\nu}_l \overline{f} \ (l \neq f)] = \sigma[\nu_l f \ (l \neq f)]. \tag{4.18}$$

Two specific limits of Eq. (4.15) are of particular interest. By taking $m_f \to 0$, the resulting cross section corresponds to elastic neutrino scattering on light leptons. This approximation is very good for $f = \{e, \mu\}$. In this case, Eq. (4.15) reduces to

$$\lim_{m_f \to 0} \sigma[\nu_l f \ (f \neq l)] = \frac{G_F^2 s}{3\pi} \Big[g_V^2 + g_A^2 + g_V g_A \Big], \tag{4.19}$$

where we have dropped the supercript f for the fermions. Another interesting scenario is the limit $E_{\mathrm{LAB}}/m_f \ll 1$. The physical interpretation of such a limit is neutrino scattering on heavy fermions, *e.g.* protons, where the resulting recoil energy of the fermion is small. Imposing this limit on Eq. (4.15), one finds that

$$\lim_{E_{\mathrm{LAB}}/m_f \ll 1} \sigma[\nu_l f \ (f \neq l)] = \frac{G_F^2 E_{\mathrm{LAB}}^2}{\pi} \Big[g_V^2 + 3 g_A^2 \Big]. \tag{4.20}$$

Eq. (4.20) agrees with the result of Ref. [23], which proposes elastic neutrino-proton scattering for detection of supernova neutrinos.

Fig. 4.4 contains a plot of Eq. (4.15) for the most common fermion scattering components on Earth, $f = e, n, p$. The respective coupling constants are summarized in Tab. 2.3, where the quark terms are used to construct the nucleon coupling constants through $g_V^p = 2g_V^u + g_V^d$, $g_A^p = 2g_A^u + g_A^d$ and $g_V^n = g_V^u + 2g_V^d$, $g_A^n = g_A^u + 2g_A^d$. [1]

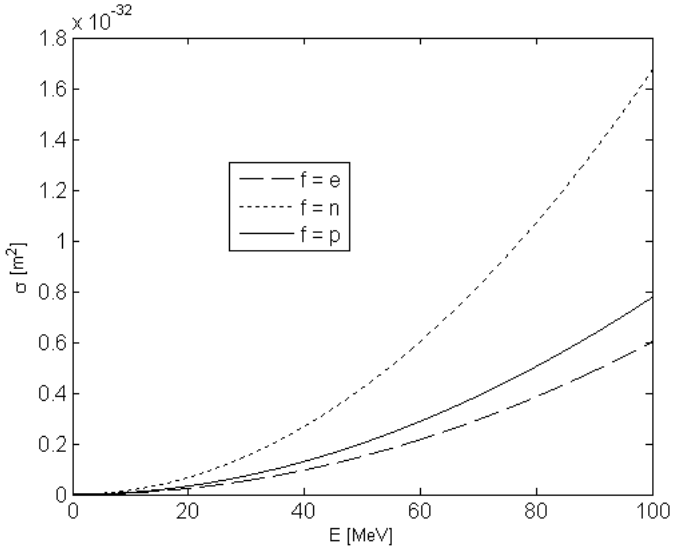


Figure 4.4: The elastic neutrino-fermion scattering cross section Eq. (4.15) for $f = e, n, p$ as a function of the CM neutrino kinetic energy E.

4.1.2 Charged current scattering

Having derived the general expression Eq. (4.15) for elastic neutrino-fermion scattering processes mediated by the Z boson, we can now include the case $f = l$. This process is mediated by the W boson in addition to Z, thus providing Feynman diagrams as shown in Fig. 4.5. The

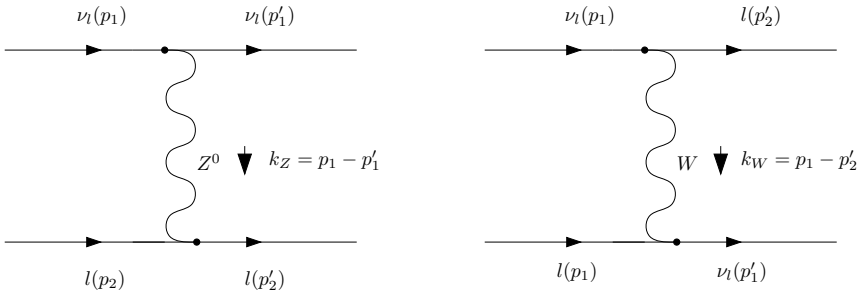


Figure 4.5: Lowest contributing order Feynman diagrams for $\nu_l + l \to \nu_l + l$.

[1] Note that this is a truth with modifications for g_A^p and g_A^n, due to the axial current anomaly (see *e.g.* Peskin & Schröder [14] chapter 19) that leads to adjusted values for the axial vector coupling constants for nucleons.

total Feynman amplitude in the low-energy limit $k^2 \ll \{m_Z^2, m_W^2\}$ is now $\mathcal{M} = \mathcal{M}_Z + \mathcal{M}_W$, where

$$\begin{aligned}\mathcal{M}_Z &= \frac{-2\mathrm{i}G_F}{\sqrt{2}}\overline{u}_{\nu_l}(1')[\gamma^\alpha(g_V^{\nu_l} - g_A^{\nu_l}\gamma_5)]u_{\nu_l}(1)\overline{u}_l(2')[\gamma_\alpha(g_V^l - g_A^l\gamma_5)]u_l(2),\\ \mathcal{M}_W &= \frac{-\mathrm{i}G}{\sqrt{2}}\overline{u}_l(2')[\gamma^\alpha(1-\gamma_5)]u_{\nu_l}(1)\overline{u}_{\nu_l}(1')[\gamma_\alpha(1-\gamma_5)]u_l(2).\end{aligned} \tag{4.21}$$

By using the Fierz identity [2]

$$\overline{u}_1[\gamma^\alpha(1-\gamma_5)]u_2\overline{u}_3[\gamma_\alpha(1-\gamma_5)]u_4 = \overline{u}_1[\gamma^\alpha(1-\gamma_5)]u_4\overline{u}_3[\gamma_\alpha(1-\gamma_5)]u_2 \tag{4.22}$$

for arbitrary spinors u_i, $\mathcal{M}_W$ obtains the same sequence of spinors as $\mathcal{M}_Z$. This leaves us with

$$\mathcal{M} = \frac{-2\mathrm{i}G}{\sqrt{2}}\overline{u}_{\nu_l}(1')\Big[\gamma^\alpha(g_V^{\nu_l} - g_A^{\nu_l}\gamma_5)\Big]u_{\nu_l}(1)\overline{u}_l(2')\Big[\gamma_\alpha[(g_V^l+1) - (g_A^l+1)\gamma_5]\Big]u_l(2). \tag{4.23}$$

This is exactly the amplitude Eq. (4.4) with the replacements $g_V^f \to g_V^l + 1$, $g_A^f \to g_A^l + 1$. We are immediately able to write down the total cross section for elastic $\nu_l l$ scattering, namely

$$\sigma[\nu_l l] = \lim_{\substack{g_V^f \to g_V^l + 1\\ g_A^f \to g_A^l + 1}} \sigma[\nu_l f \ (l \neq f)]. \tag{4.24}$$

4.2 Matter potentials

Restricting ourselves to two neutrino flavors, the vacuum Hamiltonian in mass eigenstate space reads $H_0^{\text{mass}} = \text{diag}(E_1, E_2)$. We transform to flavor space by performing $H_0^{\text{flav}} = UH_0^{\text{mass}}U^{-1}$, where U is the mixing matrix from Eq. (3.8). The MSW-effect is included by taking into account neutrino interactions with the W and Z bosons. The induced matter effects are added to H, producing

$$H = H_0 + H_Z^n + H_Z^p + H_Z^e + H_Z^\mu + H_W^e + H_W^\mu. \tag{4.25}$$

Here, $H_Z^i = \text{diag}(V_Z^i, V_Z^i)$ with $i \in \{n, p, e, \mu\}$, $H_W^e = \text{diag}(V_W^e, 0)$, and $H_W^\mu = \text{diag}(0, V_W^\mu)$, omitting the notation $^{\text{flav}}$ for quantities in flavor space from now on. The superscript refers to the scattering component while the subscript indicates which gauge boson mediates the reaction, i.e. neutral or charged current. For example, V_Z^μ represents the effective matter potential due to neutral current scattering on muons.

The diagonal form of the neutral current Hamiltonians is due to the fact that both neutrino flavors are equally affected by this potential. On the other hand, the charged current Hamiltonians only affect one of the neutrino flavors, dependent on the scattering component. For instance, it is clear that while a ν_e feels a charged current potential due to scattering on electrons, a ν_μ does not.

[2] See *e.g.* Mandl & Shaw [10] chapter 14.

4.2.1 Derivation of V_Z^n and V_W^e

First, we seek the quantity

$$V_W^e = \langle \nu_e(p_1, s_1) e(p_2, s_2) | H_W | \nu_e(p_1, s_1) e(p_2, s_2) \rangle, \tag{4.26}$$

where H_W is the charged current contribution due to scattering on electrons. Since we are dealing with elastic scattering, it is fair to assume that the neutrinos and electrons conserve their momentum as shown in Eq. (4.26). From Eq. (2.9), we immediately write down the low-energy Hamiltonian density relevant for $\nu_e e$ scattering

$$\mathcal{H}_W(x) = \frac{G_F}{\sqrt{2}} \big[\overline{e}(x)\gamma^\beta(1-\gamma_5)\nu_e(x)\big]\big[\overline{\nu}_e(x)\gamma_\beta(1-\gamma_5)e(x)\big], \tag{4.27}$$

omitting the superscript $^{\text{eff}}$ for clarity. Naïve insertion of this density into

$$H_W = \int_V \mathcal{H}_W(x) \mathrm{d}\mathbf{x}, \tag{4.28}$$

is not correct. The presence of electrons in a medium leads to two important modifications. First of all, the statistical energy distribution of the electrons in the medium is accounted for by integration over the Fermi function $f(E_e, T)$ which is normalized to $\int f(E_e, T)\mathrm{d}\mathbf{p}_e = 1$. Secondly, since we do not know the polarization of the electrons, an averaging over spins $1/2\sum_s$ is needed. In total, this corresponds to transforming Eq. (4.27) to

$$\mathcal{H}_W(x) = \int f(E_e, T)\frac{G_F}{\sqrt{2}} \times \frac{1}{2}\sum_{s_2} \big[\overline{e}(x)\gamma^\beta(1-\gamma_5)\nu_e(x)\big]\big[\overline{\nu}_e(x)\gamma_\beta(1-\gamma_5)e(x)\big]\mathrm{d}\mathbf{p}_2. \tag{4.29}$$

Since only electrons with $(p, s) = (p_2, s_2)$ will contribute to Eq. (4.26), we obtain

$$\begin{aligned}
&\big[\overline{e}(x)\gamma^\beta(1-\gamma_5)\nu_e(x)\big]\big[\overline{\nu}_e(x)\gamma_\beta(1-\gamma_5)e(x)\big]|\nu_e(p_1, s_1)e(p_2, s_2)\rangle \\
&\qquad = \frac{1}{2VE_2(p_2)}\big[a^\dagger_{s_2}(\mathbf{p}_2)a_{s_2}(\mathbf{p}_2)\overline{u}_{s_2}(p_2)\gamma^\beta(1-\gamma_5)\nu_e(x)\big] \\
&\qquad\qquad \times \big[\overline{\nu}_e(x)\gamma_\beta(1-\gamma_5)u_{s_2}(p_2)\big]|\nu_e(p_1, s_1)e(p_2, s_2)\rangle.
\end{aligned} \tag{4.30}$$

Making the identification of the number operator $\mathrm{Num}_{s_2}(\mathbf{p}_2) = a^\dagger_{s_2}(\mathbf{p}_2)a_{s_2}(\mathbf{p}_2)$, insertion of Eq. (4.30) into Eq.(4.26) produces

$$\begin{aligned}
V_W^e = \langle \nu_e(p_1, s_1)e(p_2, s_2)|\frac{G_F}{4\sqrt{2}V} \times \int\int f(E_e, T)\sum_{s_2}\frac{\mathrm{Num}_{s_2}(\mathbf{p}_2)}{E_e(\mathbf{p}_2)}\big[\overline{u}_{s_2}(p_2)\gamma^\beta(1-\gamma_5)\nu_e(x)\big] \\
\times \big[\overline{\nu}_e(x)\gamma_\beta(1-\gamma_5)u_{s_2}(p_2)\big]\mathrm{d}\mathbf{x}\ \mathrm{d}\mathbf{p}_2|\nu_e(p_1, s_1)e(p_2, s_2)\rangle.
\end{aligned} \tag{4.31}$$

It should be clear that the $\nu_e(x)$ and $\overline{\nu}_e(x)$ symbols refer to the second quantized fields from Eq. (2.8), while $|\nu_e(p_i, s_i)\rangle$, $i = 1, 2$, simply are representations for neutrinos with 4-momentum p_i and spin s_i. In order to continue without too many complications, assume that the material is isotropic and holds an equal number of electrons with spin up as spin down,

i.e. a non-magnetic material. This leads to

$$\begin{aligned} V_W^e &= \langle \nu_e(p_1,s_1)e(p_2,s_2)|\frac{G_F}{4\sqrt{2}} \times \int\int \frac{f(E_e,T)N_e(\mathbf{p}_2)}{E_e(\mathbf{p}_2)} \sum_{s_2} \big[\overline{u}_{s_2}(p_2)\gamma^\beta(1-\gamma_5)\nu_e(x)\big] \\ &\quad \times \big[\overline{\nu}_e(x)\gamma_\beta(1-\gamma_5)u_{s_2}(p_2)\big]\mathrm{d}\mathbf{x}\ \mathrm{d}\mathbf{p}_2|\nu_e(p_1,s_1)e(p_2,s_2)\rangle \\ &= \langle \nu_e(p_1,s_1)e(p_2,s_2)|\frac{G_F}{4\sqrt{2}} \times \int\int \frac{f(E_e,T)N_e(\mathbf{p}_2)}{E_e(\mathbf{p}_2)} \overline{\nu}_e(x)\gamma_\beta(1-\gamma_5)\nu_e(x) \\ &\quad \times \sum_{s_2} \big[\overline{u}_{s_2}(p_2)\gamma^\beta(1-\gamma_5))u_{s_2}(p_2)\big]\mathrm{d}\mathbf{x}\ \mathrm{d}\mathbf{p}_2|\nu_e(p_1,s_1)e(p_2,s_2)\rangle. \end{aligned} \tag{4.32}$$

Here, we have used the Fierz identity Eq. (4.22) on arbitrary spinors $\{u_i\}$ to re-arrange the ν_e and e spinors in a fashion that makes it possible to extract the neutrino-spinor part from the summation over s_2. The remaining sum is evaluated by

$$\begin{aligned} \sum_{s_2} \big[\overline{u}_{s_2}(p_2)\gamma^\beta(1-\gamma_5)u_{s_2}(p_2)\big] &= \mathrm{Tr}\{(\not{p}_2 + m_e)\gamma^\beta(1-\gamma_5)\} \\ &= p_{2\alpha}\mathrm{Tr}\{\gamma^\alpha\gamma^\beta(1-\gamma_5)\} = 4p_2^\beta, \end{aligned} \tag{4.33}$$

using standard relations for γ-matrices. Eq. (4.33) in synthesis with (4.32) leads to

$$\begin{aligned} V_W^e &= \langle \nu_e(p_1,s_1)e(p_2,s_2)|\frac{G_F}{\sqrt{2}} \times \int\int \frac{f(E_e,T)N_e(\mathbf{p}_2)}{E_e(\mathbf{p}_2)} \\ &\quad \times \overline{\nu}_e(x)\gamma_\beta(1-\gamma_5)\nu_e(x)p_2^\beta \mathrm{d}\mathbf{x}\ \mathrm{d}\mathbf{p}_2|\nu_e(p_1,s_1)e(p_2,s_2)\rangle \\ &= \langle \nu_e(p_1,s_1)e(p_2,s_2)|\frac{G_F N_e}{\sqrt{2}} \times \int \overline{\nu}_e(x)\gamma_0(1-\gamma_5)\nu_e(x)\mathrm{d}\mathbf{x}|\nu_e(p_1,s_1)e(p_2,s_2)\rangle, \end{aligned} \tag{4.34}$$

where we have exploited the isotropy $\int \mathbf{p}_2 f(E_e,T)\ \mathrm{d}\mathbf{p}_2 = 0$ and the expression for the total electron density $\int f(E_e,T)N_e(\mathbf{p}_2)\ \mathrm{d}\mathbf{p}_2 = N_e$. Only integration over $\mathbf{x}$ remains, such that we obtain

$$\begin{aligned} V_W^e &= \langle \nu_e(p_1,s_1)e(p_2,s_2)|\frac{G_F N_e}{\sqrt{2}} \times \int \overline{\nu}_e(x)\gamma_0(1-\gamma_5)\nu_e(x)\mathrm{d}\mathbf{x}|\nu_e(p_1,s_1)e(p_2,s_2)\rangle \\ &= \langle \nu_e(p_1,s_1)e(p_2,s_2)|\frac{G_F N_e}{\sqrt{2}} \times \frac{1}{2VE_{\nu_e}} \int \mathrm{Tr}\{(\not{p}_{\nu_e} + m_{\nu_e})\gamma^0(1-\gamma^5)\} \\ &\quad \times \overbrace{a_{s_1}^\dagger(\mathbf{p}_1)a_{s_1}(\mathbf{p}_1)}^{\mathrm{Num}_{s_1}(\mathbf{p}_1)}\mathrm{d}\mathbf{x}|\nu_e(p_1,s_1)e(p_2,s_2)\rangle \\ &= \langle \nu_e(p_1,s_1)e(p_2,s_2)|\frac{G_F N_e}{\sqrt{2}} \times \frac{1}{2VE_{\nu_e}} \int 4E_{\nu_e}\mathrm{d}\mathbf{x}|\nu_e(p_1,s_1)e(p_2,s_2)\rangle. \end{aligned} \tag{4.35}$$

Assuming normalized state vectors $|\nu_e(p_1,s_1)e(p_2,s_2)\rangle$, Eq. (4.35) reduces to

$$V_W^e = \frac{G_F N_e}{\sqrt{2}} \times \frac{2}{V}\int \mathrm{d}\mathbf{x}\langle \nu_e(p_1,s_1)e(p_2,s_2)||\nu_e(p_1,s_1)e(p_2,s_2)\rangle = \sqrt{2}G_F N_e. \tag{4.36}$$

Note that $\overline{\nu}_e e$ scattering would reverse the sign of $V_W^e(x)$, since $H_W(x) \to -H_W(x)$ in this case. Let us show this. For $\overline{\nu}_e e$ scattering, we must calculate the expectation value

$$\overline{V}_W^e(x) = \langle \overline{\nu}_e(p_1,s_1)e(p_2,s_2)|H_W^e|\overline{\nu}_e(p_1,s_1)e(p_2,s_2)\rangle. \tag{4.37}$$

The procedure is identical to the case of $\nu_e e$ up to Eq. (4.35). There, we are confronted with

$$\overline{V}^e_W = \langle \overline{\nu}_e(p_1,s_1)e(p_2,s_2)|\frac{G_F N_e}{\sqrt{2}} \times \int \overline{\nu}_e(x)\gamma_0(1-\gamma_5)\nu_e(x)\mathrm{d}\mathbf{x}|\overline{\nu}_e(p_1,s_1)e(p_2,s_2)\rangle. \quad (4.38)$$

This gives an extra minus sign compared to V^e_W, and here is why. In the general case, the operator part of this expression takes the form

$$\langle 0|b_\nu(\mathbf{p})\Big[\sum_{\mathbf{k},\mathbf{k}'} b_\nu(\mathbf{k})b^\dagger_\nu(\mathbf{k}')\Big]b^\dagger_\nu(\mathbf{p}')|0\rangle, \quad (4.39)$$

where the sum over $b_\nu(\mathbf{k})b^\dagger_\nu(\mathbf{k}')$ comes from the second quantized fields $\overline{\nu}_e(x)\nu_e(x)$. Using the canonical commutation relation $[b_\nu(\mathbf{k}), b^\dagger_\nu(\mathbf{k}')]_+ = \delta(\mathbf{k}'-\mathbf{k})$ for fermions, Eq. (4.39) becomes

$$-\langle 0|b_\nu(\mathbf{p})\Big[\sum_{\mathbf{k},\mathbf{k}'} b^\dagger_\nu(\mathbf{k}')b_\nu(\mathbf{k})\Big]b^\dagger_\nu(\mathbf{p}')|0\rangle. \quad (4.40)$$

The only non-vanishing contribution from this term is obtained by taking $\mathbf{k}=\mathbf{p}', \mathbf{k}'=\mathbf{p}$. In our case of elastic scattering, we then impose the limit $\mathbf{p}\to\mathbf{p}'$. Now it is evident from where the relative minus sign comes. Using this treatment on Eq. (4.38) produces

$$\begin{aligned}\overline{V}^e_W &= \langle \overline{\nu}_e(p_1,s_1)e(p_2,s_2)|\frac{G_F N_e}{\sqrt{2}} \times \frac{1}{2VE_{\nu_e}}\int \mathrm{Tr}\{(\not{p}_{\nu_e} - m_{\nu_e})\gamma^0(1-\gamma^5)\} \\ &\quad \times \overbrace{[-b^\dagger_{s_1}(\mathbf{p}_1)b_{s_1}(\mathbf{p}_1)]}^{\text{-Num}_{s_1}(\mathbf{p}_1)}\mathrm{d}\mathbf{x}|\overline{\nu}_e(p_1,s_1)e(p_2,s_2)\rangle \\ &= -\langle \overline{\nu}_e(p_1,s_1)e(p_2,s_2)|\frac{G_F N_e}{\sqrt{2}} \times \frac{1}{2VE_{\nu_e}}\int 4E_{\nu_e}\mathrm{d}\mathbf{x}|\overline{\nu}_e(p_1,s_1)e(p_2,s_2)\rangle. \end{aligned} \quad (4.41)$$

Demanding normalized state vectors $|\overline{\nu}_e(p_1,s_1)e(p_2,s_2)\rangle$, Eq. (4.41) reduces to

$$\overline{V}^e_W = -\frac{G_F N_e}{\sqrt{2}} \times \frac{2}{V}\int \mathrm{d}\mathbf{x}\langle \overline{\nu}_e(p_1,s_1)e(p_2,s_2)||\overline{\nu}_e(p_1,s_1)e(p_2,s_2)\rangle = -\sqrt{2}G_F N_e. \quad (4.42)$$

Comparing Eq. (4.42) to Eq. (4.36), it is clear that $\overline{V}^e_W = -V^e_W$.

We now set out to find V^n_Z due to $\nu_\alpha n$, $\alpha = e,\mu,\tau$ scattering. This reaction is mediated by the Z boson, so we must use the effective Hamiltonian density Eq. (2.10). Now, the neutron consists of one u and two d. The u part of the Hamiltonian is then

$$\frac{G_F}{2\sqrt{2}}\big[\overline{u}(x)\gamma^\mu(1-\gamma_5-\frac{8}{3}\sin^2\theta_W)u(x)\big]\big[\overline{\nu}_\alpha(x)\gamma_\mu(1-\gamma_5)\nu_\alpha(x)\big], \quad (4.43)$$

while the d part is

$$-\frac{G_F}{2\sqrt{2}}\big[\overline{d}(x)\gamma^\mu(1-\gamma_5-\frac{4}{3}\sin^2\theta_W)d(x)\big]\big[\overline{\nu}_\alpha(x)\gamma_\mu(1-\gamma_5)\nu_\alpha(x)\big]. \quad (4.44)$$

These contributions are to be added in the ratio 1:2 to obtain the relevant Hamiltonian for $\nu_e n$ scattering. In total, this gives

$$\begin{aligned}&\frac{G_F}{2\sqrt{2}}\Big[\overline{\psi}_n\gamma^\mu\big[(1-\gamma_5-\frac{8}{3}\sin^2\theta_W) - 2\times(1-\gamma_5-\frac{4}{3}\sin^2\theta_W)\big]\psi_n\Big]\Big[\overline{\nu}_\alpha(x)\gamma_\mu(1-\gamma_5)\nu_\alpha(x)\Big] \\ &\qquad = -\frac{G_F}{2\sqrt{2}}\big[\overline{\psi}_n\gamma^\mu(1-\gamma_5)\psi_n\big]\big[\overline{\nu}_\alpha(x)\gamma_\mu(1-\gamma_5)\nu_\alpha(x)\big]. \end{aligned} \quad (4.45)$$

We are left with the effective Hamiltonian

$$\mathcal{H}_Z(x) = -\frac{G_F}{2\sqrt{2}} \int f(E_n, T) \times \frac{1}{2} \sum_s \big[\overline{\psi}_n(x)\gamma^\mu(1-\gamma_5)\psi_n(x)\big] \times \big[\overline{\nu}_\alpha(x)\gamma_\mu(1-\gamma_5)\nu_\alpha(x)\big] \mathrm{d}\mathbf{p}_n. \tag{4.46}$$

Here, we have introduced the statistical Fermi distribution for neutrons $f(E_n, T)$ and summation over the neutron spins due to the assumption of unpolarized medium, just as for the electrons. We see that Eq. (4.46) is of the same form as Eq. (4.29) if we use the earlier mentioned Fierz identity, such that the rest of the analysis is equivalent to the derivation of V_W^e. Following the same procedure as above, we find

$$\begin{aligned} V_Z^n &= -\langle \nu_\alpha(p_1,s_1)n(p_2,s_2)| \frac{G_F N_n}{2\sqrt{2}} \times \int \overline{\nu}_\alpha(x)\gamma_0(1-\gamma_5)\nu_\alpha(x)\mathrm{d}\mathbf{x}|\nu_\alpha(p_1,s_1)n(p_2,s_2)\rangle \\ &= -\langle \nu_\alpha(p_1,s_1)n(p_2,s_2)| \frac{G_F N_n}{2\sqrt{2}} \times \frac{1}{2VE_{\nu_\alpha}} \int \mathrm{Tr}\{(\not{p}_{\nu_\alpha} + m_{\nu_\alpha})\gamma^0(1-\gamma^5)\} \\ &\quad \times \overbrace{a_{s_1}^\dagger(\mathbf{p}_1)a_{s_1}(\mathbf{p}_1)}^{\mathrm{Num}_{s_1}(\mathbf{p}_1)} \mathrm{d}\mathbf{x}|\nu_\alpha(p_1,s_1)n(p_2,s_2)\rangle \\ &= -\langle \nu_\alpha(p_1,s_1)n(p_2,s_2)| \frac{G_F N_n}{2\sqrt{2}} \times \frac{1}{2VE_{\nu_\alpha}} \int 4E_{\nu_\alpha}\mathrm{d}\mathbf{x}|\nu_\alpha(p_1,s_1)n(p_2,s_2)\rangle. \end{aligned} \tag{4.47}$$

With normalized state vectors $|\nu_\alpha(p_1,s_1)n(p_2,s_2)\rangle$, Eq. (4.47) leads to

$$V_Z^n = -\frac{G_F N_n}{2\sqrt{2}} \times \frac{2}{V} \int \mathrm{d}\mathbf{x}\langle \nu_\alpha(p_1,s_1)n(p_2,s_2)||\nu_\alpha(p_1,s_1)n(p_2,s_2)\rangle = -\frac{G_F N_n}{\sqrt{2}}. \tag{4.48}$$

4.2.2 Derivation of V_Z^p and V_Z^e

The axial and vector coupling constants were treated in Sec. 2.3. As it turns out, the contributions to $\mathcal{M}$ from the electron and proton exactly cancel eachother. We see this from the fact that $g_V^{\mathrm{TOT}} = g_V^{(e)} + 2g_V^{(u)} + g_V^{(d)} = 0$, and $g_A^{\mathrm{TOT}} = g_A^{(e)} + 2g_A^{(u)} + g_A^{(d)} = 0$, leaving us with only the neutron contribution to the scattering of neutrinos of arbitrary flavor [3]. However, this is only valid if the electron and proton densities in the medium are equal. Let us prove this.

The claim is that $V_Z^p + V_Z^e = 0$ when $N_e = N_p$. Now, the expression for V_Z^e is found by including the relevant terms from Eq. (2.10), which for $\nu_e e$ scattering reads

$$-\frac{G_F}{2\sqrt{2}}\big[\overline{\nu}_e(x)\gamma^\mu(1-\gamma_5)\nu_e(x)\big]\big[\overline{e}(x)\gamma^\mu(1-\gamma_5-4\sin^2\theta_W)e(x)\big]. \tag{4.49}$$

Taking into account the Fermi distribution of electrons and the averaging of spins, the expression for $V_Z^e(x)$ takes the form

$$\mathcal{H}_Z(x) = -\frac{G_F}{2\sqrt{2}} \int f(E_e, T) \times \frac{1}{2} \sum_s \big[\overline{\nu}_e(x)\gamma^\mu(1-\gamma_5)\nu_e(x)\big] \times \big[\overline{e}(x)\gamma_\mu(1-\gamma_5-4\sin^2\theta_W)e(x)\big] \mathrm{d}\mathbf{p}_e. \tag{4.50}$$

[3] As pointed out earlier, the axial current anomaly modifies the value of g_A^p, such that the total coupling constant g_A^{TOT} does not vanish. However, the vector current is conserved. Therefore, since the potentials V_Z^e and V_Z^p turn out to be proportional to their respective vector coupling constants g_V^e and g_V^p, the axial coupling is irrelevant when proving that the potentials cancel eachother.

As before, the rest of the analysis is equivalent to the derivation of V_W^e. Analogous to Eq. (4.35), it is found that

$$\begin{aligned}
V_Z^e &= -\langle\nu_e(p_1,s_1)e(p_2,s_2)|\frac{G_F N_e}{2\sqrt{2}}\times\int(1-4\sin^2\theta_W)\overline{\nu}_\alpha(x)\gamma_0 \\
&\quad\times(1-\gamma_5)\nu_\alpha(x)\mathrm{d}\mathbf{x}|\nu_e(p_1,s_1)e(p_2,s_2)\rangle \\
&= -\langle\nu_\alpha(p_1,s_1)e(p_2,s_2)|\frac{G_F N_e}{2\sqrt{2}}\times\frac{1}{2VE_{\nu_e}}\int(1-4\sin^2\theta_W)\mathrm{Tr}\{(\not{p}_{\nu_e}+m_{\nu_e})\gamma^0(1-\gamma^5)\} \\
&\quad\times\overbrace{a_{s_1}^\dagger(\mathbf{p}_1)a_{s_1}(\mathbf{p}_1)}^{\mathrm{Num}_{s_1}(\mathbf{p}_1)}\mathrm{d}\mathbf{x}|\nu_e(p_1,s_1)e(p_2,s_2)\rangle \\
&= -\langle\nu_e(p_1,s_1)e(p_2,s_2)|\frac{G_F N_e}{2\sqrt{2}}\times\frac{1}{2VE_{\nu_e}}\int(1-4\sin^2\theta_W) \\
&\quad\times 4E_{\nu_e}\mathrm{d}\mathbf{x}|\nu_e(p_1,s_1)e(p_2,s_2)\rangle. \qquad (4.51)
\end{aligned}$$

Demanding normalized state vectors $|\nu_e(p_1,s_1)n(p_2,s_2)\rangle$, Eq. (4.51) leads to

$$\begin{aligned}
V_Z^e &= -\frac{G_F N_e}{2\sqrt{2}}\times\frac{2}{V}(1-4\sin^2\theta_W)\int\mathrm{d}\mathbf{x}\langle\nu_e(p_1,s_1)e(p_2,s_2)||\nu_e(p_1,s_1)e(p_2,s_2)\rangle \\
&= -\frac{G_F(1-4\sin^2\theta_W)N_e}{\sqrt{2}}. \qquad (4.52)
\end{aligned}$$

In order to derive V_Z^p, we attack the problem in the same way as for V_Z^n. A proton consists of two u and one d quarks, so the total contribution to the proton is seen to be

$$\begin{aligned}
&\frac{G_F}{2\sqrt{2}}\Big[\overline{\psi}_p\gamma^\mu\big[2\times(1-\gamma_5-\frac{8}{3}\sin^2\theta_W)-(1-\gamma_5-\frac{4}{3}\sin^2\theta_W)\big]\psi_p\Big]\Big[\overline{\nu}_\alpha(x)\gamma_\mu(1-\gamma_5)\nu_\alpha(x)\Big] \\
&\qquad = \frac{G_F}{2\sqrt{2}}\big[\overline{\psi}_p\gamma^\mu(1-\gamma_5-4\sin^2\theta_W)\psi_p\big]\big[\overline{\nu}_\alpha(x)\gamma_\mu(1-\gamma_5)\nu_\alpha(x)\big], \qquad (4.53)
\end{aligned}$$

when adding Eqs. (4.43) and (4.44) in the ratio 2:1, and including the extra overall factor 2 due to the double quark contribution from Eq. (2.10). This gives the effective Hamiltonian for $\nu_\alpha p$, $\alpha = e,\mu,\tau$ scattering, namely

$$\begin{aligned}
\mathcal{H}_Z(x) = \frac{G_F}{2\sqrt{2}}\int f(E_p,T)\times\frac{1}{2}\sum_s\big[\overline{\psi}_p(x)\gamma^\mu(1-\gamma_5-4\sin^2\theta_W)\psi_p(x)\big] \\
\times\big[\overline{\nu}_\alpha(x)\gamma_\mu(1-\gamma_5)\nu_\alpha(x)\big]\mathrm{d}\mathbf{p}_n. \qquad (4.54)
\end{aligned}$$

The further analysis is then just as for V_W^e, and leads to

$$\begin{aligned}
V_Z^p &= -\langle\nu_\alpha(p_1,s_1)p(p_2,s_2)|\frac{G_F N_p}{2\sqrt{2}}\times\int(1-4\sin^2\theta_W)\overline{\nu}_\alpha(x)\gamma_0 \\
&\quad\times(1-\gamma_5)\nu_\alpha(x)\mathrm{d}\mathbf{x}|\nu_\alpha(p_1,s_1)p(p_2,s_2)\rangle \\
&= \langle\nu_\alpha(p_1,s_1)p(p_2,s_2)|\frac{G_F N_p}{2\sqrt{2}}\times\frac{1}{2VE_{\nu_\alpha}}\int(1-4\sin^2\theta_W)\mathrm{Tr}\{(\not{p}_{\nu_\alpha}+m_{\nu_\alpha})\gamma^0(1-\gamma^5)\} \\
&\quad\times\overbrace{a_{s_1}^\dagger(\mathbf{p}_1)a_{s_1}(\mathbf{p}_1)}^{\mathrm{Num}_{s_1}(\mathbf{p}_1)}\mathrm{d}\mathbf{x}|\nu_\alpha(p_1,s_1)p(p_2,s_2)\rangle \\
&= \langle\nu_\alpha(p_1,s_1)p(p_2,s_2)|\frac{G_F N_p}{2\sqrt{2}}\times\frac{1}{2VE_{\nu_\alpha}}\int(1-4\sin^2\theta_W) \\
&\quad\times 4E_{\nu_\alpha}\mathrm{d}\mathbf{x}|\nu_\alpha(p_1,s_1)p(p_2,s_2)\rangle. \qquad (4.55)
\end{aligned}$$

As before, we require the state vectors $|\nu_\alpha(p_1,s_1)p(p_2,s_2)\rangle$ to be normalized. Eq. (4.55) then gives

$$\begin{aligned}
V_Z^p &= \frac{G_F N_p}{2\sqrt{2}}\times\frac{2}{V}(1-4\sin^2\theta_W)\int\mathrm{d}\mathbf{x}\langle\nu_\alpha(p_1,s_1)p(p_2,s_2)||\nu_\alpha(p_1,s_1)p(p_2,s_2)\rangle \\
&= \frac{G_F N_p(1-4\sin^2\theta_W)}{\sqrt{2}}. \qquad (4.56)
\end{aligned}$$

From Eqs. (4.52) and (4.56) it is easily seen that

$$V_Z^e + V_Z^p\Big|_{N_e=N_p} = 0. \qquad (4.57)$$

Thus, there is no effective matter potential felt by neutrinos due to scattering on protons and electrons mediated by Z in an electrically neutral medium.

4.2.3 Derivation of V_Z^μ and V_W^μ

Since Earth contains practically no μ particles, $N_\mu \simeq 0$, and the terms $\{V_Z^\mu, V_W^\mu\}$ are set to zero. This means that the only effective potentials felt by the ν_e and ν_μ neutrinos travelling through Earth are V_Z^n and V_W^e, due to scattering of ν_e and ν_μ on neutrons and the scattering of ν_e on electrons, respectively.

We summarize our results in Tab. 4.1. A more comprehensive list of neutrino matter potentials can be found in *e.g.* Ref. [24]. Generalization to matter potentials for ν_τ-scattering should be trivial. The upper sign refer to neutrinos, while the lower gives the matter potential for antineutrinos.

4.2.4 Potential strength comparison

To get an impression of how strong these matter potentials are, consider Fig. 4.6. The graph has been produced from Tab. 4.1 by assuming an electrically neutral medium, such that

$$G_F N_e = G_F N_n = G_F N_p = 2.67\times10^{-14}\times\rho[\mathrm{g/cm^3}]. \qquad (4.58)$$

Table 4.1: Neutrino matter potentials.

Type of reaction	Matter potential
V_Z^n	$\mp G_F N_n/\sqrt{2}$
V_Z^p	$\pm G_F(1-4\sin^2\theta_W)N_p/\sqrt{2}$
V_Z^e	$\mp G_F(1-4\sin^2\theta_W)N_e/\sqrt{2}$
V_Z^μ	$\mp G_F(1-4\sin^2\theta_W)N_\mu/\sqrt{2}$
V_W^e	$\pm 2G_F N_e/\sqrt{2}$
V_W^μ	$\pm 2G_F N_\mu/\sqrt{2}$

Thus, one finds that for instance $V_W^e[\text{eV}] = \sqrt{2}\times 2.67\times 10^{-14}\times\rho[\text{g/cm}^3]$. As is seen from the figure, realistic densities give rise to very weak interaction potentials. The charged current contribution from scattering on electrons is $\mathcal{O}(10^{-13})$ eV, compared to the upper mass limit $m_{\nu_e}\simeq 3$ eV from Tab. 2.2. The MSW-effect is thus very small for normal Earth conditions.

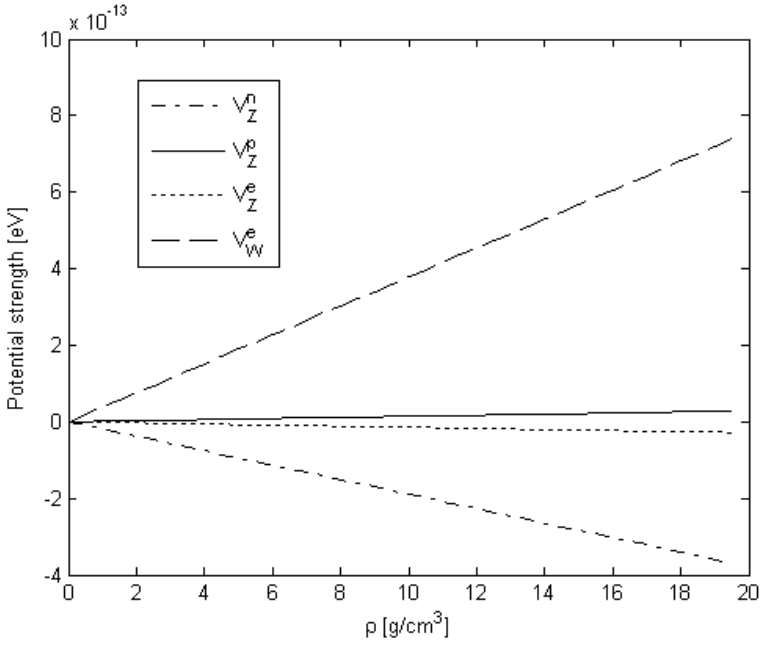


Figure 4.6: Induced matter potentials from Earth.

4.3 MSW-effect for constant electron density

Now, the equation of motion for neutrinos in matter is

$$\mathrm{i}\frac{\mathrm{d}}{\mathrm{d}t}\begin{bmatrix}\nu_e\\ \nu_\mu\end{bmatrix} = H\begin{bmatrix}\nu_e\\ \nu_\mu\end{bmatrix}. \tag{4.59}$$

In the previous section, we proved that the only non-vanishing contributions from Earth to the matter potential were V_Z^n and V_W^e. However, H_Z^n in Eq. (4.25) is not relevant for neutrino

oscillations since it is proportional to the identity matrix $\mathbf{I}$. This means all flavors will be equally affected by the neutral current contribution. Such a common phase factor can be disregarded with respect to oscillations. H_W^e, on the other hand, will only affect the electron neutrinos, thus shifting the balance in their favor. The equation of motion then explicitely reads

$$\mathrm{i}\frac{\mathrm{d}}{\mathrm{d}t}\begin{bmatrix}\nu_e\\ \nu_\mu\end{bmatrix} = \left[\frac{1}{2E}\begin{bmatrix} m_1^2c_\theta^2 + m_2^2s_\theta^2 & c_\theta s_\theta(m_2^2-m_1^2)\\ c_\theta s_\theta(m_2^2-m_1^2) & m_1^2s_\theta^2+m_2^2c_\theta^2\end{bmatrix} + \begin{bmatrix}\sqrt{2}G_FN_e & 0\\ 0 & 0\end{bmatrix}\right]\begin{bmatrix}\nu_e\\ \nu_\mu\end{bmatrix}. \quad (4.60)$$

Using basic trigonometric relations and designating $\Delta m^2 = m_2^2 - m_1^2$, $\Sigma m^2 = m_2^2 + m_1^2$, and $\mathcal{N} = 2\sqrt{2}G_FN_eE/\Delta m^2$, Eq. (4.60) is rewritten to

$$\mathrm{i}\frac{\mathrm{d}}{\mathrm{d}t}\begin{bmatrix}\nu_e\\ \nu_\mu\end{bmatrix} = \frac{1}{4E}\left[(\Sigma m^2 + \Delta m^2\mathcal{N})\mathbf{I} + \Delta m^2\begin{bmatrix}\mathcal{N}-c_{2\theta} & s_{2\theta}\\ s_{2\theta} & -\mathcal{N}+c_{2\theta}\end{bmatrix}\right]\begin{bmatrix}\nu_e\\ \nu_\mu\end{bmatrix}.$$

Suppose now that the flavor states in matter are described by a set of new mass eigenstates $\{\nu_1^m, \nu_2^m\}$, obtained through

$$\begin{bmatrix}\nu_e\\ \nu_\mu\end{bmatrix} = \overbrace{\begin{bmatrix}c_{\theta_m} & s_{\theta_m}\\ -s_{\theta_m} & c_{\theta_m}\end{bmatrix}}^{U_m}\begin{bmatrix}\nu_1^m\\ \nu_2^m\end{bmatrix}.$$

If so, the modified amplitude term in matter $\mathcal{A}_m$ will be obtained simply by substituting $\theta \to \theta_m$ in Eq. (3.9). The pursuit of θ_m begins by demanding that U_m diagonalizes our Hamiltonian with the result

$$U_m^{-1}HU_m = \begin{bmatrix}H^+ & 0\\ 0 & H^-\end{bmatrix}, \quad (4.61)$$

where

$$H^\pm = \frac{(\Sigma m^2 + \Delta m^2\mathcal{N}) \mp \Delta m^2\sqrt{(\mathcal{N}-c_{2\theta})^2 + s_{2\theta}^2}}{4E}. \quad (4.62)$$

The calculation of θ_m is straight-forward but tedious, and we shall make do with the result

$$s_{2\theta_m}^2 = \frac{s_{2\theta}^2}{s_{2\theta}^2 + (\mathcal{N}-c_{2\theta})^2}. \quad (4.63)$$

We see that $\theta = \theta_m$ in the case of $N_e = 0$, i.e. vacuum, as would be expected for consistency. Now, the oscillation term $\mathcal{W}$ is also affected by the presence of matter through a shift of mass eigenvalues. This means we must make the replacement $\Delta m^2 \to \Delta M^2$ in Eq. (3.9) where M_i are the mass eigenvalues for neutrinos in matter. These are given by $M_1^2 = 2EH^+$ and $M_2^2 = 2EH^-$. The total transformation from vacuum scenario to presence of matter is thus obtained by substituting the vacuum parameters with their matter equivalents, i.e. $\theta \to \theta_m$ and $\Delta m^2 \to \Delta M^2$, for the case of a constant electron density. Performing these operations on Eq. (3.9) results in the total oscillation probability for neutrinos traversing through matter $P^{\mathrm{MSW}}_{\nu_e\to\nu_\mu}(t) = s_{2\theta_m}^2\sin^2(\Delta M^2t/4E) = \mathcal{A}_m\mathcal{W}_m$. Explicitely, this reads

$$P^{\mathrm{MSW}}_{\nu_e\to\nu_\mu}(t) = \frac{s_{2\theta}^2}{s_{2\theta}^2 + (\mathcal{N}-c_{2\theta})^2} \times \sin^2\frac{t\Delta m^2\sqrt{s_{2\theta}^2 + (\mathcal{N}-c_{2\theta})^2}}{4E} \quad (4.64)$$

This result tells us how the oscillation probability is modified for the MSW-effect. Eq. (4.64) was first derived by Wolfenstein in 1978 (see Ref. [22]), but with the wrong sign on the matter potential.

The mixing between neutrinos becomes maximal when $\theta_m = \pi/4$ since this leads to $\mathcal{A}_m = 1$. The resonance condition is then $\mathcal{N} = c_{2\theta}$, which means that there exists a resonance density N_e for a given neutrino energy E and square mass difference Δm^2. This is readily seen from Fig. 4.7, where the maximum value of the oscillation probability in a medium $[P^{\text{MSW}}_{\nu_e \to \nu_\mu}(t)]_{\max} = \mathcal{A}_m$ is plotted against $\mathcal{N}$.

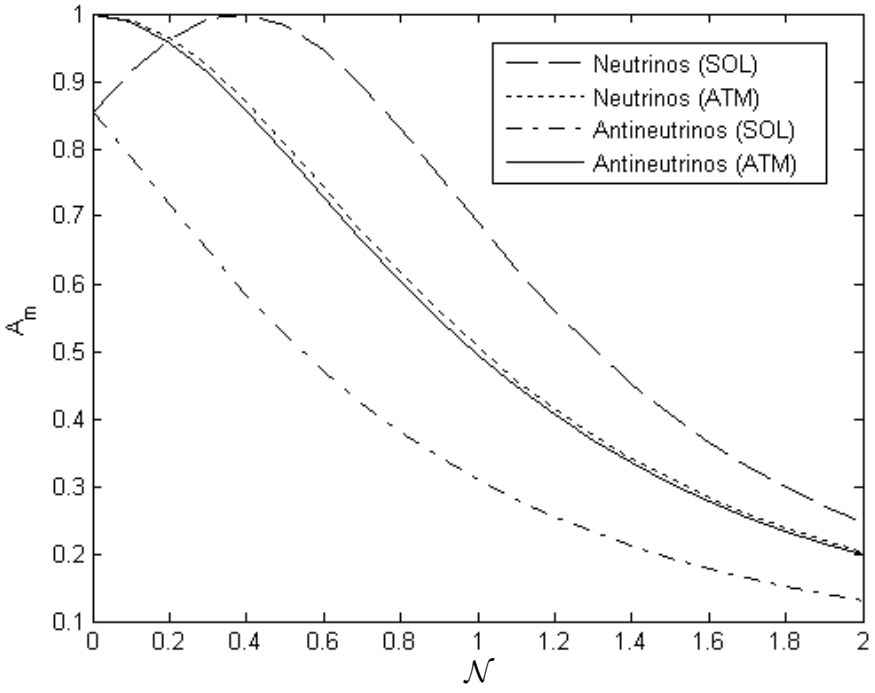


Figure 4.7: Plot of $\mathcal{A}_m$ against $\mathcal{N}$ for neutrinos and antineutrinos, using both solar and atmospheric best-fit parameters. The resonance condition is never met for two-flavor antineutrino oscillations, but is very close for atmospheric best-fit mixing parameters.

Chapter 5

Exploiting step-wise density shifts

The case of an electron density behaving like a unit-step function is of practical importance since it models a very realistic situation, and has been studied in *e.g.* Refs. [25, 26]. Take for instance accelerator neutrinos propagating through air and eventually hitting a solid detector. The electron density is then exactly of the type described by a unit-step function, with an abrupt shift at the boundary between air and detector.

5.1 Single unit-step density profile

We begin by rewinding our analysis from Sec. 4.3 back to Eq. (4.59), where the time dependence of the electron density must be taken into account. The situation being considered is illustrated in Fig. 5.1.

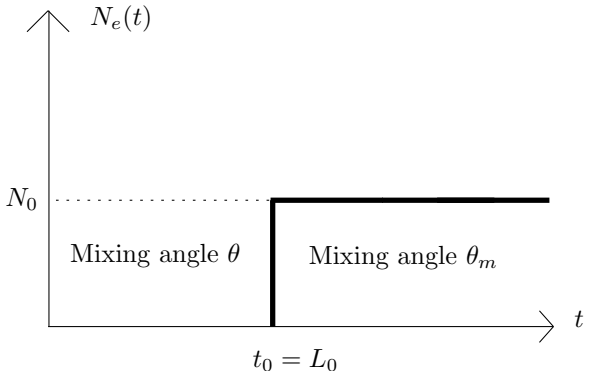


Figure 5.1: Neutrino transition from vacuum to a constant non-zero electron density modelled by a unit-step function.

Our electron density is now described by

$$N_e(t) = N_0 \times \Theta(t - L_0), \tag{5.1}$$

where N_0 is the electron density in the medium, L_0 is the baseline length traversed by the neutrinos before hitting the slab of material, and $\Theta(t - L_0)$ is an ordinary unit-step function. Such an abrupt shift in electron density is certainly non-adiabatic, and corresponds to a

momentous change in mixing angles and mass eigenvalues for the neutrino eigenstates. The question is how the phase information of the neutrino eigenstates is translated through the shift of $N_e(t)$. Can one assume that the phase information of $\mathcal{W}$ is conserved in the transition between vacuum and matter, such that the neutrinos "remember" the how far they have traveled? Mathematically, this means that $\mathcal{W}$ would transform as

$$\sin^2 \frac{t\Delta m^2}{4E} \to \sin^2 \frac{t\Delta M^2}{4E} \tag{5.2}$$

across the material slab at $t = t_0$. If the neutrinos instead "forget" their history up to t_0, time would effectively reset and the transformation would look like

$$\sin^2 \frac{t\Delta m^2}{4E} \to \sin^2 \frac{(t-t_0)\Delta M^2}{4E}. \tag{5.3}$$

It is also possible that the solution is neither of these transformations, and consists of a mixture of both. So let us investigate this. As pointed out in Ref. [6], the flavor eigenstates must be continuous in the transition between vacuum and a massive medium even if the density change is extremely non-adiabatic, i.e. abrupt. Since the flavor states are coupled to the mass eigenstates through Eq. (3.8), this condition reads

$$\begin{bmatrix} c_\theta & s_\theta \\ -s_\theta & c_\theta \end{bmatrix} \begin{bmatrix} |\nu_1(\mathbf{x},0)\rangle \mathrm{e}^{-\mathrm{i}E_1 t_0} \\ |\nu_2(\mathbf{x},0)\rangle \mathrm{e}^{-\mathrm{i}E_2 t_0} \end{bmatrix} = \begin{bmatrix} c_{\theta_m} & s_{\theta_m} \\ -s_{\theta_m} & c_{\theta_m} \end{bmatrix} \begin{bmatrix} |\nu_{1m}(\mathbf{x},0)\rangle \\ |\nu_{2m}(\mathbf{x},0)\rangle \end{bmatrix}. \tag{5.4}$$

We seek to express the new mass eigenstates $|\nu_{im}(\mathbf{x},0)\rangle$ in terms of the old $|\nu_i(\mathbf{x},0)\rangle$. Straightforward matrix multiplication leads to the equations

$$\begin{aligned} \nu_{1m} &= \nu_1\big[c_\theta c_{\theta_m} + s_\theta s_{\theta_m}\big]\mathrm{e}^{-\mathrm{i}E_1 t_0} + \nu_2\big[s_\theta c_{\theta_m} - c_\theta s_{\theta_m}\big]\mathrm{e}^{-\mathrm{i}E_2 t_0} \\ \nu_{2m} &= \nu_1\big[c_\theta s_{\theta_m} - s_\theta c_{\theta_m}\big]\mathrm{e}^{-\mathrm{i}E_1 t_0} + \nu_2\big[s_\theta s_{\theta_m} + c_\theta c_{\theta_m}\big]\mathrm{e}^{-\mathrm{i}E_2 t_0}, \end{aligned} \tag{5.5}$$

where we have shortened down the notation to $|\nu_{im}(\mathbf{x},0)\rangle \equiv \nu_{im}$. We are ready to compute the oscillation probability $\widetilde{P}_{\nu_\alpha \to \nu_\beta}$ given by Eq. (3.4), where the tilde represents our special case of the non-adiabatic transition from $\theta \to \theta_m$. In the general case, we start off with a neutrino of flavor α at $t = 0$ and ask the question: *What is the probability to measure a ν_β at $t \geq t_0$, given that the neutrino in question is a ν_α at $t = 0$?*

Now, the α-flavor in vacuum and β-flavor in matter are described by

$$\begin{aligned} |\nu_\alpha(\mathbf{x},t)\rangle &= c_\theta \nu_1 \mathrm{e}^{-\mathrm{i}E_1 t} + s_\theta \nu_2 \mathrm{e}^{-\mathrm{i}E_2 t}, \quad t \leq t_0 \\ |\nu_\beta(\mathbf{x},t)\rangle &= -s_\theta \nu_{1m} \mathrm{e}^{-\mathrm{i}E_{1m}(t-t_0)} + c_\theta \nu_{2m} \mathrm{e}^{-\mathrm{i}E_{2m}(t-t_0)}, \quad t \geq t_0. \end{aligned}$$

The probability for a flavor conversion from α to β after the neutrino has crossed the density shift at $t = t_0$ is then given by

$$\begin{aligned} \widetilde{P}_{\nu_\alpha \to \nu_\beta}(t,t_0) &= |\langle \nu_\alpha(\mathbf{x},0) | \nu_\beta(\mathbf{x},t)\rangle|^2 \\ &= \big|\langle c_\theta \nu_1 + s_\theta \nu_2| \\ &\quad - s_{\theta_m} \nu_{1m} \mathrm{e}^{-\mathrm{i}E_{1m}(t-t_0)} + c_{\theta_m} \nu_{2m} \mathrm{e}^{-\mathrm{i}E_{2m}(t-t_0)}\rangle\big|^2, \quad t \geq t_0. \end{aligned} \tag{5.6}$$

Inserting the new mass eigenstates from Eq. (5.5) together with the orthogonality condition Eq. (3.6) leads to

$$\begin{aligned}\widetilde{P}_{\nu_\alpha\to\nu_\beta}(t,t_0) = a_1^2 + a_2^2 + a_3^2 + a_4^2 + 2(a_1a_2 + a_3a_4)\cos\Big[\frac{\Delta m^2 t_0}{2E}\Big] \\ + 2(a_1a_3 + a_2a_4)\cos\Big[\frac{\Delta M^2(t-t_0)}{2E}\Big] \\ + 2a_1a_4\cos\Big[\frac{\Delta M^2(t-t_0)}{2E} + \frac{\Delta m^2 t_0}{2E}\Big] \\ + 2a_2a_3\cos\Big[\frac{\Delta M^2(t-t_0)}{2E} - \frac{\Delta m^2 t_0}{2E}\Big], \quad t \geq t_0,\end{aligned} \tag{5.7}$$

where we have introduced the constants

$$\begin{aligned}a_1 &= -c_\theta s_{\theta_m}\big[c_\theta c_{\theta_m} + s_\theta s_{\theta_m}\big], \quad a_2 = -s_\theta s_{\theta_m}\big[s_\theta c_{\theta_m} - c_\theta s_{\theta_m}\big] \\ a_3 &= c_\theta c_{\theta_m}\big[c_\theta s_{\theta_m} - s_\theta c_{\theta_m}\big], \quad a_4 = s_\theta c_{\theta_m}\big[s_\theta s_{\theta_m} + c_\theta c_{\theta_m}\big].\end{aligned} \tag{5.8}$$

For consistency, we should have

$$\widetilde{P}_{\nu_\alpha\to\nu_\beta}(t=t_0,t_0) = P_{\nu_\alpha\to\nu_\beta}(t_0) \tag{5.9}$$

for all θ. Above, $P_{\nu_\alpha\to\nu_\beta}(t_0)$ is the ordinary vacuum oscillation probability from Eq. (3.9). Here, the reader is spared for the details of this criteria since it involves a nightmare of trigonometic identities, but Eq. (5.9) can be shown to hold for all θ.

5.1.1 A study of $\widetilde{P}_{\nu_\alpha\to\nu_\beta}(t,t_0)$

To get an impression of how Eq. (5.7) behaves, consider Fig. 5.2. Here, L_p designates the distance where the vacuum oscillation probability Eq. (3.9) reaches its first maximum $\mathcal{W}=1$, i.e. $L_\mathrm{p} = 2\pi E/\Delta m^2$.

As is seen from the plot, there is hardly any distinction between $\widetilde{P}_{\nu_\alpha\to\nu_\beta}$ and $P_{\nu_\alpha\to\nu_\beta}$ right after the density shift. On a larger scale, the picture is quite different. Here, $\widetilde{P}_{\nu_\alpha\to\nu_\beta}$ actually reaches unity after a sufficiently large interval for $\theta_m = \pi/4$. An interesting observation of the results in Fig. 5.2 is that there is a significant difference between the vacuum oscillation probability and the equivalent in matter after a certain interval, dependent on where L_0 is chosen. This could be exploited to obtain experimental restrictions upon the mixing parameters $\{\Delta m^2, \theta\}$. We shall discuss this idea in detail later on.

For $L_0 \geq L_\mathrm{p}$, the presence of a non-adiabatic density shift is seen to enhance the oscillation probability immediately after the shift. Now, the mixing angle θ_m in the medium is in general a function of several parameters such as kinetic energy E and electron density N_e. In the following section, we study the density dependence of the mixing angle to understand what kind of materials that are required in order to enhance oscillation probabilities.

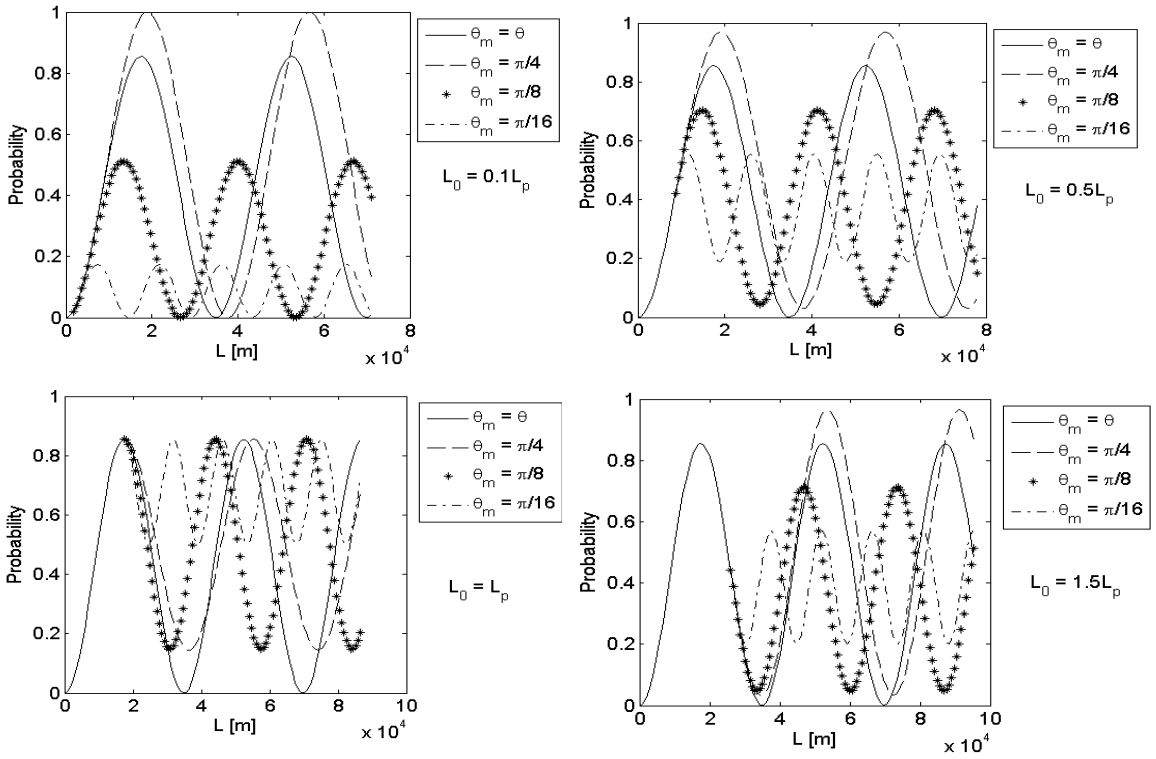


Figure 5.2: Eq. (3.9) compared to Eq. (5.7) for solar neutrino parameters. $E = 1$ MeV has been chosen as a representative for this species. Comparison is shown for several values of L_0.

5.1.2 Mass density vs. mixing angle

Recall Eq. (4.63), which can be slightly re-written to

$$s^2_{2\theta_m} = \frac{s^2_{2\theta}}{s^2_{2\theta} + [(2\sqrt{2}G_F N_e E/\Delta m^2 - c_{2\theta})]^2}. \tag{5.10}$$

It is instructive to consider how the mixing angle depends on the total mass density ρ. In the case of an electrically neutral medium, the total mass density is given by

$$\rho = N_e \times m_e \times (\frac{m_p}{m_e} + \frac{m_n}{m_e} + \frac{m_e}{m_e}), \tag{5.11}$$

where m_p, m_n, and m_e are the proton, neutron, and electron masses, respectively. Inverting Eq. (5.10) leads to

$$\theta_m = \frac{1}{2}\arcsin\frac{s_{2\theta}}{\sqrt{s^2_{2\theta} + \left[\frac{\sqrt{2}G_F\rho E}{m_p\Delta m^2} - c_{2\theta}\right]^2}}, \tag{5.12}$$

where Eq. (5.11) has been inserted under the approximation $m_p \simeq m_n \gg m_e$. In the following, let ρ^{R} and N_e^{R} denote the resonance mass density and electron density that gives $\theta_m = \pi/4$. Fig. 5.3 shows a plot of Eq. (5.12) for solar and atmospheric neutrino parameters. Observe that the physical parameter space is spanned by $\theta_m \in [0, \pi/2]$ and $\Delta m^2 \geq 0$.

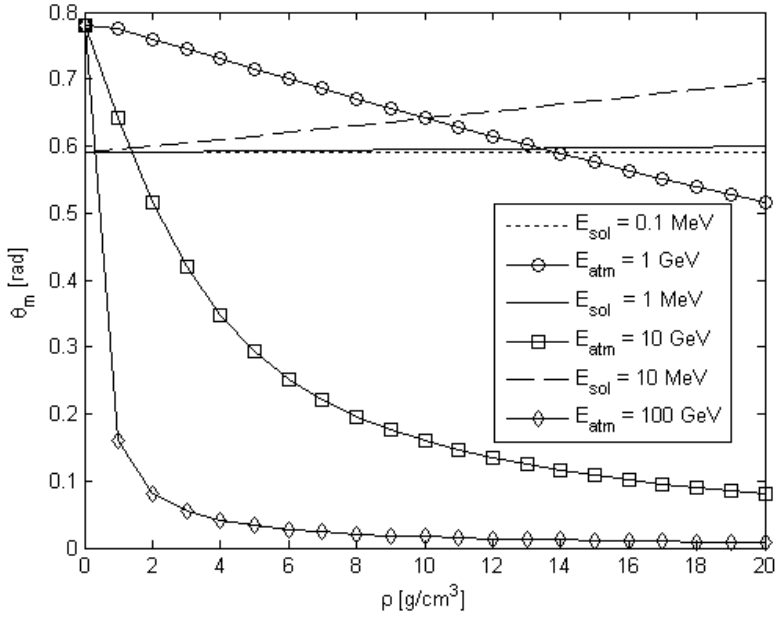


Figure 5.3: Mixing angle in medium θ_m as a function of total mass density ρ. Solar neutrino parameters $\Delta m^2_{\text{SOL}} = 7.1 \times 10^{-5}$ eV^2, $\theta^{\text{SOL}} = 0.59$ and atmospheric neutrino parameters $\Delta m^2_{\text{ATM}} = 2.5 \times 10^{-3}$ eV^2, $\theta^{\text{ATM}} = 0.78$, respectively. Resonance peak occurs at $\theta_m = \pi/4 \simeq 0.78$.

The total mass density scale does not exceed 20 g/cm^3, since the most dense material on Earth is Iridium with $\rho \simeq 22$ g/cm^3 [27]. It is clear from the plot that resonance peaks $\theta_m = \pi/4$ occur for values of ρ within the set range for the atmospheric neutrinos, while the solar neutrinos require impossible densities in order to satisfy the resonance condition.

From Fig. 5.3, we see that low densities $\rho < \rho^{\text{R}}$ correspond to small mixing angles, but never smaller than the vacuum mixing angle for the relevant species (solar or atmospheric). Larger densities $\rho > \rho^{\text{R}}$ forces θ_m down towards zero. However, the amount of material available in large quantities for detection purposes drastically reduces for each increasing unit of ρ. In an experimental setup, the mixing angle, i.e. material density, can be chosen dependent on whether one wishes to significantely enhance or decrease the oscillation probability.

An interesting opportunity arises from this study. Effectively, the modified oscillation probability for a given species of neutrinos depends on kinetic energy E, material density ρ, baseline length L_0. By placing a slab of material in the way of the neutrino beam, the oscillation probability is changed, thus altering the expected ratio of ν_α and ν_β measured behind the slab, compared to normal vacuum oscillations. This could actually be used to determine the neutrino parameters $\{\Delta m^2, \theta\}$ to an even higher accuracy. By comparing the flux ratio $F_{\nu_\alpha}/F_{\nu_\beta}$ with and without a slab of material in front of the detector, information could be acquired concerning these mixing parameters. This idea will recieve further attention in Sec. 6.1.

5.2 Neutrino propagators

We can use a more instructive approach in order to derive Eq. (5.7). Consider the flavor state vector $|\Psi(\mathbf{x},t)\rangle$ describing the neutrino. Our initial condition is that

$$|\Psi(\mathbf{x},0)\rangle = \begin{bmatrix} 1 \\ 0 \end{bmatrix}, \tag{5.13}$$

using a basis where

$$|\nu_\alpha(\mathbf{x},0)\rangle = \begin{bmatrix} 1 \\ 0 \end{bmatrix} \quad |\nu_\beta(\mathbf{x},0)\rangle = \begin{bmatrix} 0 \\ 1 \end{bmatrix}. \tag{5.14}$$

The mass state vector is then given by

$$|\Psi(\mathbf{x},t)\rangle^{\text{mass}} = \begin{bmatrix} c_\theta & -s_\theta \\ s_\theta & c_\theta \end{bmatrix} |\Psi(\mathbf{x},t)\rangle = \begin{bmatrix} c_\theta \\ s_\theta \end{bmatrix}. \tag{5.15}$$

Since the mass eigenstates have a time-dependence through the exponential factor $\exp(-\mathrm{i}E_i t)$, we can write the flavor state vector as $|\Psi(\mathbf{x},t)\rangle = \mathcal{K}(t_0)|\Psi(\mathbf{x},0)\rangle$, where the propagator $\mathcal{K}(t_0)$ is defined by

$$\mathcal{K}(t) = \begin{bmatrix} c_\theta & s_\theta \\ -s_\theta & c_\theta \end{bmatrix} \begin{bmatrix} \mathrm{e}^{-\mathrm{i}E_1 t} & 0 \\ 0 & \mathrm{e}^{-\mathrm{i}E_2 t} \end{bmatrix} \begin{bmatrix} c_\theta & -s_\theta \\ s_\theta & c_\theta \end{bmatrix}. \tag{5.16}$$

Up to the point t_0, our treatment is analogous to the vacuum case. Demanding that the flavor eigenstate is contineous across the density shift, we write

$$|\Psi(\mathbf{x},t_0)\rangle^{\text{mass}} = \begin{bmatrix} c_{\theta_m} & -s_{\theta_m} \\ s_{\theta_m} & c_{\theta_m} \end{bmatrix} |\Psi(\mathbf{x},t_0)\rangle, \tag{5.17}$$

where the subscript m denotes our transition to a massive medium. The propagation through the medium is described by replacing the vacuum quantities with their medium equivalents, such that the flavor state vector in the medium is

$$|\Psi(\mathbf{x},t,t_0)\rangle = \mathcal{K}_m(t-t_0)\mathcal{K}(t_0)|\Psi(\mathbf{x},0)\rangle, \quad t \geq t_0. \tag{5.18}$$

Here, $\mathcal{K}_m(t-t_0)$ is defined in a similar fashion as the vacuum propagator, namely

$$\mathcal{K}_m(t) = \begin{bmatrix} c_{\theta_m} & s_{\theta_m} \\ -s_{\theta_m} & c_{\theta_m} \end{bmatrix} \begin{bmatrix} \mathrm{e}^{-\mathrm{i}E_{1m} t} & 0 \\ 0 & \mathrm{e}^{-\mathrm{i}E_{2m} t} \end{bmatrix} \begin{bmatrix} c_{\theta_m} & -s_{\theta_m} \\ s_{\theta_m} & c_{\theta_m} \end{bmatrix}. \tag{5.19}$$

This is an interesting result. Eq. (5.18) provides us with the opportunity to use the $\mathcal{K}(t)$ and $\mathcal{K}_m(t)$ propagators to "rotate" the original flavor eigenstate ν_α into a ν_β by an appropriate choice of parameters. Simply put, if we write

$$|\Psi(\mathbf{x},t,t_0)\rangle = \begin{bmatrix} A(t,t_0) \\ B(t,t_0) \end{bmatrix}, \quad t \geq t_0 \tag{5.20}$$

then a rotation to another flavor eigenstate means making $|B(t,t_0)|^2$ as large as possible, since the lower component describes the β-flavor. $B(t,t_0)$ is identified as

$$B(t,t_0) = c_{\theta_m} s_{\theta_m} \Big(\mathrm{e}^{-\mathrm{i}E_{2m}(t-t_0)} - \mathrm{e}^{-\mathrm{i}E_{1m}(t-t_0)} \Big) \Big(c^2 \mathrm{e}^{-\mathrm{i}E_1 t} + s_\theta^2 \mathrm{e}^{-\mathrm{i}E_2 t} \Big) + c_\theta s_\theta \Big(\mathrm{e}^{-\mathrm{i}E_2 t} - \mathrm{e}^{-\mathrm{i}E_1 t} \Big) \Big(c_{\theta_m}^2 \mathrm{e}^{-\mathrm{i}E_{2m}(t-t_0)} + s_{\theta_m}^2 \mathrm{e}^{-\mathrm{i}E_{1m}(t-t_0)} \Big) \tag{5.21}$$

through Eqs. (5.16), (5.18), and (5.19). The calculation of $|B(t,t_0)|^2$ is consistent with Eq. (5.7), and expresses the probability that a ν_α created at $t = 0$ would have oscillated into a ν_β at t after encountering a medium with an abrupt density shift at $t = t_0$.

5.3 Multiple step-wise density profiles

The idea of using multiple propagators for rotating the neutrino eigenstate vector is interesting in terms of detection. We wish to investigate the behaviour of the oscillation probability when using multiple step-wise density profiles, as shown in Fig. 5.4.

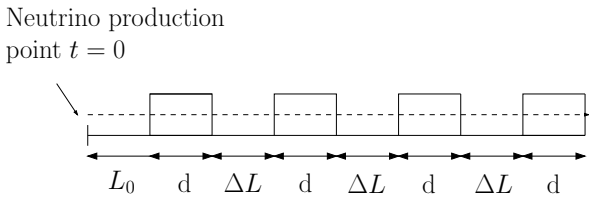


Figure 5.4: Using multiple material slabs to rotate the neutrino flavor.

Similarly to Eq. (5.18), we obtain

$$|\Psi(\mathbf{x}, L_0, \Delta L, n, d)\rangle = \mathcal{K}_{\mathrm{TOT}}(L_0, \Delta L, n, d) |\Psi(\mathbf{x}, 0)\rangle. \tag{5.22}$$

where

$$\mathcal{K}_{\mathrm{TOT}}(L_0, \Delta L, n, d) = \mathcal{K}_m(d) \times \Big[\mathcal{K}(\Delta L) \mathcal{K}_m(d) \Big]^{(n-1)} \times \mathcal{K}(L_0), \quad n = 1, 2, 3, .. \tag{5.23}$$

Hopefully, it would be possible to adjust the parameters $L_0, \Delta L, n$, and d so that the oscillation probability significantely differs from the vacuum case after a reasonable number of iterations n. A criteria for such behaviour is that the relevant neutrino species needs to have a short oscillation length both in vacuum and matter of realistic density, so that the probability varies on a sensible length scale. Solar and atmospheric neutrinos are poor candidates for such a detector setup. The oscillation length is given as the length of a cycle in the oscillation probability, i.e. the period where the argument of $\mathcal{W}$ goes from 0 to π. This means that

$$L_{\mathrm{osc}} = \frac{4E\pi}{\Delta m^2}. \tag{5.24}$$

Solar neutrinos yield typical values of $L_{\mathrm{osc}}^{\mathrm{SOL}} \simeq 10^4 - 10^5$ m, while the atmospheric type offers $L_{\mathrm{osc}}^{\mathrm{ATM}} \simeq 10^6 - 10^7$ m. Comfort is found in the LSND parameters (see Sec. 3.2) which yield $L_{\mathrm{osc}}^{\mathrm{LSND}} \simeq 10^1 - 10^2$ m. This is more to our liking, since these numbers mean that a full oscillation cycle will take place over an interval of only about 100 m.

So let us take on an analytical approach to find the conditions appropriate to rotate a neutrino flavor. Eq. (5.23) can be written

$$|\Psi(\mathbf{x}, L_0, \Delta L, n, d)\rangle = [U_m D_m(d) U_m^{-1} U D(\Delta L) U^{-1}]^{(n-1)} \times U_m D_m(d) U_m^{-1} U D(L_0) U^{-1} |\Psi(\mathbf{x}, 0)\rangle, \tag{5.25}$$

where U and U_m are the ordinary 2 x 2 mixing matrices in vacuum and the medium, while $D(x)$ $= \mathrm{diag}(1, \mathrm{e}^{-\mathrm{i}\Delta m^2 x/2E})$ and $D_m(x) = \mathrm{diag}(1, \mathrm{e}^{-\mathrm{i}\Delta M^2 x/2E})$. To obtain the diagonal matrices D and D_m, we have extracted common phase factors of the type $\mathrm{e}^{\mathrm{i}\varphi}$ which are irrelevant when pursuing the oscillation probability. The resonance $|\Psi(\mathbf{x}, L_0, \Delta L, n, d)\rangle = [0\ 1]^{\mathrm{T}}$ is obtained when we set $L_0 = \Delta L$ and choose the phases such that

$$\Delta m^2 \Delta L/2E = \Delta M^2 d/2E = \pi. \tag{5.26}$$

As a consequence, $D(\Delta L) = D_m(d) = \mathrm{diag}(1, -1)$, which results in

$$[U_m D_m(D) U_m^{-1}][U D(\Delta L) U^{-1}] = \begin{bmatrix} \cos 2(\theta_m - \theta) & \sin 2(\theta_m - \theta) \\ -\sin 2(\theta_m - \theta) & \cos 2(\theta_m - \theta) \end{bmatrix}. \tag{5.27}$$

Eq. (5.27) is thus seen to be equal to $\mathrm{e}^{2\mathrm{i}(\theta_m - \theta)\sigma^y}$, where σ^y is the Pauli matrix

$$\sigma^y = \begin{bmatrix} 0 & \mathrm{i} \\ -\mathrm{i} & 0 \end{bmatrix}. \tag{5.28}$$

Eq. (5.25) then becomes $|\Psi(\mathbf{x}, L_0, \Delta L, n, d)\rangle = \mathrm{e}^{2\mathrm{i}n(\theta_m - \theta)\sigma^y} |\Psi(\mathbf{x}, 0)\rangle$, written out as

$$|\Psi(\mathbf{x}, L_0, \Delta L, n, d)\rangle = \begin{bmatrix} \cos(2n\Delta\theta) \\ -\sin(2n\Delta\theta) \end{bmatrix}, \tag{5.29}$$

with the definition $\Delta\theta \equiv (\theta_m - \theta)$. The resonance condition for the number of iterations n is then $2n\Delta\theta = \pm\pi/2$. If this condition is met, the probability for a flavor conversion reads $\widetilde{P}_{\nu_\alpha \to \nu_\beta} = \sin^2(2n\Delta\theta) = 1$. In other words, it is possible to obtain a *complete flavor conversion for any neutrino or antineutrino species*. It is important to realize that this resonance crucially depends on choosing the phases properly. To see this, recall that d and ΔL must be chosen to satisfy Eq. (5.26). If d and L instead are slightly perturbed to satisfy $\Delta m^2 \Delta L/2(E + \Delta E) = \Delta M^2 d/2(E + \Delta E) = \pi$, the conversion probability never reaches unity and is displaced. This is shown in Fig. 5.5.

In general, the width of the resonance depends on $\Delta\theta$. For $\Delta E/E \sim \Delta\theta$, it is seen from the graph that one still gets reasonably close to the resonance. Larger values of ΔE destroys the resonance, and gives a flat curve for $\widetilde{P}_{\nu_\alpha \to \nu_\beta}$.

For solar and atmospheric best-fits $(\Delta m^2_{\mathrm{SOL}}, \theta_{\mathrm{SOL}})$ and $(\Delta m^2_{\mathrm{ATM}}, \theta_{\mathrm{ATM}})$, Eq. (5.26) would require too large lengths d and ΔL to be satisfied in an realistic detection setup. Using LSND parameters, however, it is possible to satisfy Eq. (5.26) using realistic detector dimensions of $\mathcal{O}(10^2)$ m (same order of magnitude as the oscillation length). With the material density in the range $\rho = [1, 11]$ g/cm^3, $\Delta\theta \sim 10^{-9}$, so that the resonance is very narrow. Actually, the number of iterations required to increase $\widetilde{P}_{\nu_\alpha \to \nu_\beta}$ will be very large unless there is a way of obtaining a large $\Delta\theta$ in the medium. This is challenging when restricted to realistic densities

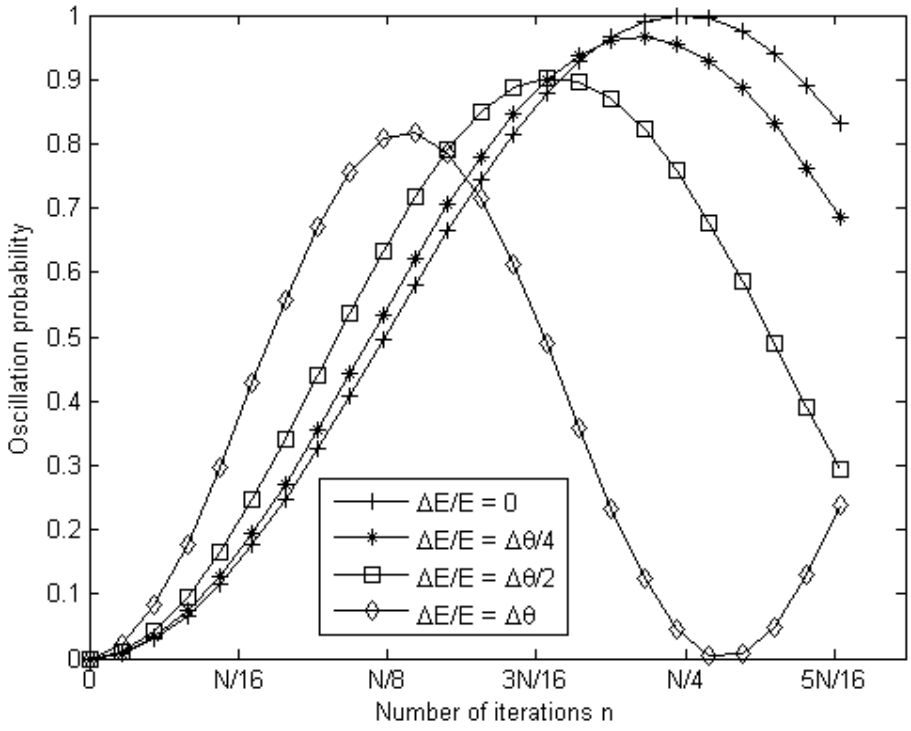


Figure 5.5: Oscillation probability for the setup in Fig. 5.4 as a function of number of iterations. n is given in units of $N = \pi/\Delta\theta$. As expected, the resonance occurs at $n = \pi/4\Delta\theta$. Material density $\rho = 1$ g/cm^3 has been used.

(see Sec. 5.1.2).

It is true that the oscillation probability in a medium can reach unity for a neutrino propagating through a single material slab of resonance density (see Eq. (4.64)). The required densities are unfortunately impossible to obtain for solar best-fit values. Antineutrinos, on the other hand, cannot meet the resonance condition $\mathcal{N} = c_{2\theta}$, since the potential sign is reversed. Our treatment of multiple non-adiabatic density shifts, however, allows for a complete conversion of one antineutrino flavor α to a flavor β, which is relevant for accelerator and reactor experiments involving antineutrino oscillations (see Secs. 6.2.5 and 6.3.1).

This analysis has shown that it is possible, in theory, to obtain a complete flavor conversion for any neutrino species by exploiting the MSW-effect for multiple non-adiabatic density shifts. Gaining an angle $\Delta\theta$ for every density shift in the oscillation probability, the final expression $\widetilde{P}_{\nu_\alpha \to \nu_\beta} = \sin^2(2n\Delta\theta)$ depends on the number of iterations n. A large $\Delta\theta$ means few iterations, but this is hard to achieve in laboratory experiments, as we have seen. In the following, we shall estimate the deviation from the vacuum oscillation probability for a single non-adiabatic density shift for specific neutrino species.

Chapter 6

Detector dimensions and coherence effects

In this chapter, we set out to investigate if it is possible to use either appearance or disappearance experiments that exploit the MSW-effect with respect to gaining additional knowledge about neutrino mixing parameters $\{\Delta m^2, \theta\}$. Using a neutrino source consisting of primarily one flavor ν_α, appearance experiments look for interactions with ν_β originally not present in the beam. Disappearance experiments look for a diminished flux of ν_α due to oscillations. The first case places a lower limit $P_{\nu_\alpha \to \nu_\beta} > P_{\text{lim}}$ on the oscillation probability, since one at best can detect all ν_β from oscillations. Similarly, the flavor conserving probability must satisfy the condition $P_{\nu_\alpha \to \nu_\alpha} < 1 - P_{\text{lim}}$ in the second case.

Using these conditions gives an allowed region of mixing parameters $\{\Delta m^2, \theta\}$ that are consistent with the experiments. In theory, one should obtain additional constraints on the mixing parameters by exploiting the MSW-effect on the neutrinos as they interact with matter, which we studied in chapter 5. This could be done by comparing the fluxes with and without a slab of material in front of the detector. But as previously mentioned, this argument depends upon whether the distinction between $P_{\nu_\alpha \to \nu_\beta}$ and $\widetilde{P}_{\nu_\alpha \to \nu_\beta}$ is sufficiently large. Let us find out.

6.1 Statistical analysis

Here, we quite simply ask the question: *What kind of dimension is required for a massive structure in front of a neutrino detector in order to produce a statistically significant difference between the oscillation probability in vacuum and matter?*

Let Φ^0_α designate the ν_α flux at a neutrino source. The flux of ν_β at the detector site is then given as $\Phi_\beta = P_{\alpha\beta}\Phi^0_\alpha$, where we have shortened down our notation to $P_{\nu_\alpha \to \nu_\beta} \to P_{\alpha\beta}$. If we place matter in front of the detector, an appearance experiment will measure a flux of $\widetilde{\Phi}_\beta$ at the detector site. The difference in flux between the vacuum and matter case reads

$$\Delta\Phi_\beta = \Phi_\beta - \widetilde{\Phi}_\beta = (P_{\alpha\beta} - \widetilde{P}_{\alpha\beta})\Phi^0_\alpha. \tag{6.1}$$

In a disappearance experiment, the difference in the ν_α flux is $\Delta\Phi_\alpha = \Delta P_{\alpha\alpha}\Phi^0_\alpha$, with $\Delta P_{\alpha\alpha}$

$\equiv P_{\alpha\alpha} - \widetilde{P}_{\alpha\alpha}$. Of course, the measured flux quantitites are subject to statistical uncertainties, due to the non-exact nature of detection. If one is to obtain any significant results, i.e. measurable $\Delta\Phi$, these uncertainties must not exceed the magnitude of the flux deviation.

To illustrate how the concept is meant to work, consider the following example. A neutrino detector site is able to measure the solar neutrino flux of ν_e to an accuracy of $\pm a$. During a disappearance experiment, the flux without any interference of material prior the detector is found to be $\Phi_\alpha = A \pm a$. The flux at the neutrino source is assumed to be known from theoretical studies, say $\Phi_\alpha^0 = A_0 \pm a_0$. When placing a material slab of length d at a baseline lengths L_0, the neutrino flux at the detector is altered to $\widetilde{\Phi}_\alpha = \widetilde{A} \pm a$. Note that we are operating with the same statistical uncertainty a in both cases. Thus, one obtains the conditions

$$\frac{\Delta\Phi_\alpha(L_0^i + d^i)}{\Phi_\alpha^0} = \Delta P_{\alpha\alpha}(L_0^i + d^i), \quad i = 1, 2, 3.. \tag{6.2}$$

for every baseline length L_0^i and material slab length d^i. $\Delta\Phi_\alpha(L_0^i + d^i)$ must be found from direct measurements of fluxes with and without the slab of material, each with its own statistical uncertainty. Combining all of these arguments leads to the expression

$$\frac{[A(L_0^i + d^i) - \widetilde{A}(L_0^i + d^i)] \pm 2a}{A_0 \pm a_0} = \Delta P_{\alpha\alpha}(L_0^i + d^i), \quad i = 1, 2, 3.. \tag{6.3}$$

Since $\Delta P_{\alpha\alpha}$ depends on the neutrino mixing parameters, the measured fluxes will give rise to restrictions on these quantities. Experiments would thus provide an allowed parameter region in the $(\Delta m^2, \sin^2 2\theta)$-plane. Remember that $P_{\alpha\alpha}$ and $\widetilde{P}_{\alpha\alpha}$ are given by Eqs. (3.9) and (5.7).

Consider the following hypothetical experimental scenario. Neutrinos with $E \sim 1$ MeV emanate from a nuclear reactor due to neutron decay, and travel a length of L_0 before they encounter an abrupt density shift. The medium has a given density ρ and a length d. For these parameters, a contour plot of $\Delta P_{e\mu}$ (assuming $\overline{\nu}_e \leftrightarrow \overline{\nu}_\mu$ oscillations) is shown in Fig. 6.1.

Assume that the experimental data yields

$$\frac{[A(L_0 + d) - \widetilde{A}(L_0 + d)] \pm 2a}{A_0 \pm a_0} = 0.29 \pm 0.09 \tag{6.4}$$

for the measured and theoretical fluxes $A, \widetilde{A}$, and A_0. Then, the allowed parameter region for the neutrino mixing parameters is found by localizing the corresponding region in Fig. 6.1. In our case, the allowed region is in the neighborhood of the darkest patch at $\Delta m^2 \sim 10^{-4}$. By varying L and d, one would obtain additional contour plots with allowed regions that give consistency between theory and experiment. The union of these contour plots then pinpoints $\{\Delta m^2, \theta\}$ down to a higher accuracy.

Of course, this crude analysis only serves as a simple introduction to how the presence of a non-adiabatic density shift can be exploited in terms of determining the mixing parameters. In the following sections, we investigate exactly how good results one can achieve using realistic parameters for detection setups. But before doing so, we need to say a few words about neutrino coherence.

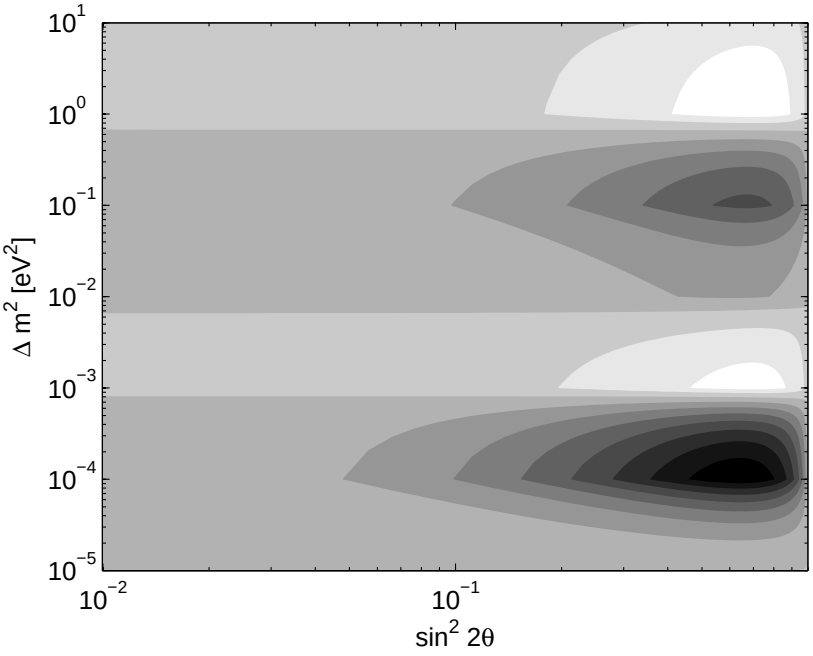


Figure 6.1: Contour plot of $\Delta P_{e\mu}$ in the $(\Delta m^2, \sin^2 2\theta)$-plane for our hypothetical parameter set $\{L_0, d, \rho\}$. Each contour line represents 5% increase for darker regions, and a 5% decrease for brighter regions. The asymptotic lines close to $\Delta m^2 = 10^0$, 10^{-2}, and 10^{-3} eV^2 give $\Delta P_{e\mu} = 0$.

6.2 Neutrino coherence

We defined the oscillation length in Sec. 5.3 by setting the argument of $\mathcal{W}$ in Eq. (3.9) equal to π, which marks the beginning of a new cycle. The coherence of a neutrino beam is determined by the energy spread ΔE of the neutrinos. If ΔE is large, then some of the neutrinos will undergo significantly less oscillations than the rest, as seen when substituting E with $E + \Delta E$ in Eq. (3.9). As a result, it gets tougher to extract oscillation patterns at an observation site, since the arriving neutrinos will be incoherent.

6.2.1 General arguments

Imagine a ν_e created in some weak interaction, for instance in the sun. At $t = 0$, this neutrino consists of a certain linear combination between the mass eigenstates $|\nu_i\rangle$, represented as wave packets. Since these eigenstates have different masses m_i, the corresponding wave packets will propagate with different velocities. This means that the original ν_e-packet will disperse as time goes, and that the mass eigenstate wave packets will eventually be spatially separated, as illustrated in Fig. 6.2. Oscillations should be lost at the point of separation, meaning an observer would have a constant probability of detecting the incoming wave packets as a given flavor state. This corresponds to averaging out the oscillation term in Eq. (3.9), leaving us with

$$P_{\nu_\alpha \to \nu_\beta} = \frac{1}{L_{\text{osc}}} \int_0^{L_{\text{osc}}} \sin^2(2\theta) \times \sin^2 \frac{L\Delta m^2}{4E} \mathrm{d}L = \frac{1}{2} \sin^2(2\theta) \tag{6.5}$$

and $P_{\nu_\alpha \to \nu_\alpha} = 1 - \frac{1}{2}\sin^2(2\theta)$ for two-flavor oscillations.

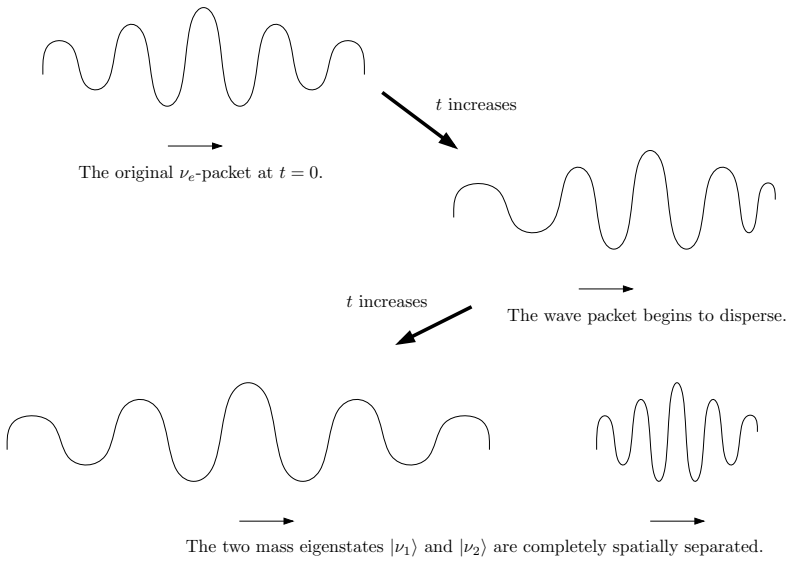


Figure 6.2: The dispersion of the original ν_e wave packet at $t = 0$ into the two mass eigenstates $|\nu_1\rangle$ and $|\nu_2\rangle$.

One way of defining the coherence length of the neutrino beam is found in Ref. [28], where L_{coh} is the distance where a neutrino with energy E has oscillated one more time than a neutrino with energy $E + \Delta E$. This means that

$$\frac{L_{\text{coh}}\Delta m^2 + 4\pi E}{4E} = \frac{L_{\text{coh}}\Delta m^2}{4(E + \Delta E)}. \tag{6.6}$$

Solving Eq. (6.6) for the coherence length yields $L_{\text{coh}} = L_{\text{osc}}\frac{E}{\Delta E}$. Using practical units, we express the coherence length as

$$L_{\text{coh}} = \frac{2.48E^2(\text{MeV})}{\Delta m^2(\text{eV}^2)\Delta E(\text{MeV})}. \tag{6.7}$$

L_{coh} is the distance from the neutrino source where the mass eigenstates that made up the original wave packet have been spatially separated, thus no longer interfering and causing oscillations.

There can be more than one cause of a neutrino energy spread, thus leading to a corresponding number of coherence lengths. The shortest of these coherence length will determine the effective L_{coh}. It is necessary to analyze the various sources of energy spread in a neutrino beam to find the effective coherence length. The authors of Ref. [29] point out the following possible sources for the energy spread ΔE:

- Uncertainties in energy measurements for neutrinos interacting with a detector.
- Uncertainties related to the life-time of the neutrino-producing particle, *e.g.* a muon.

- Uncertainties related to the energy and momentum of the neutrino at the production point due to quantum-mechanical effects.

Our somewhat naïve interpretation of the coherence length deserves a comment. As pointed out in Ref. [28], the accuracy ε to which we can measure the energy of an incoming neutrino is of significance when discussing coherence. Now, we just stated that when the mass eigenstates constituting the wave packet become spatially separated after traveling a distance L_{coh}, all oscillations will be lost. Although this argument seems valid at first consideration, it is not quite accurate and here is why. If the detector can measure the neutrino energy to an accuracy ε, the time interval required for a measurement is $t \sim \frac{1}{\varepsilon}$. One can see this from the Heisenberg principle of uncertainty $\varepsilon t \sim 1/2$. This means that even though the eigenstates are spatially separated and arrive at different times, an oscillation would still be observed if the slowest eigenstates arrives within the time interval it takes to do the measurement.

Let us solidify this argument quantitatively and see exactly which conditions that must be fulfilled in order for oscillations to be detected even if the mass eigenstates are spatially separated. Consider a ν_α produced at $t = 0$. The flavor state is a superposition of the mass eigenstates as described in Sec. 3.1. The mass eigenstates propagate with different velocities due to their different masses, and thus arrive at our detector at different times t_i. If the mass eigenstate $|\nu_i\rangle$ is detected at a time t_i, and an oscillation has occured, the new flavor eigenstate is given as

$$|\nu_\beta(\mathbf{x}, t)\rangle = \sum_{j=1}^{3} U_{\beta j} |\nu_j(\mathbf{x}, 0)\rangle \mathrm{e}^{-\mathrm{i}E_j(t-t_j)}. \tag{6.8}$$

Thus, the flavor state can be thought of as a new superposition of mass eigenstates $|\nu_i\rangle$ that were created at $t = t_i$. It is now uncomplicated to calculate the oscillation probability

$$\begin{aligned} P_{\nu_\alpha \to \nu_\beta}(t) &= |\langle \nu_\alpha(\mathbf{x}, 0) | \nu_\beta(\mathbf{x}, t)\rangle|^2 \\ &= \left| \sum_{i=1}^{3} \sum_{j=1}^{3} U_{\alpha i} U^*_{\beta j} \delta_{ij} \exp\Big[\mathrm{i}[E_j(t - t_j) - E_i(t - t_i)]\Big] \right|^2 \end{aligned} \tag{6.9}$$

For clarity, we continue with the two-flavor scenario. Eq. (6.9) then reduces to

$$\begin{aligned} P_{\nu_\alpha \to \nu_\beta}(t) &= \sin^2 2\theta \times \sin^2 \Big[\frac{E_2(t - t_2) - E_1(t - t_1)}{2}\Big] \\ &= \sin^2 2\theta \times \sin^2 \Big[\frac{(E_2 - E_1)t - E_2 t_2 + E_1 t_1}{2}\Big] \end{aligned} \tag{6.10}$$

The coherent expression for oscillation probability Eq. (3.9) is regained if the condition $E_2 t_2 = E_1 t_1$ is met. This can be written as $(E + m_2^2/2E)t_2 = (E + m_1^2/2E)t_1$ when taking neutrino masses as small compared to the momentum E. As a result, we obtain

$$|t_2 - t_1| = \Big|\frac{\Delta m^2 L_0}{2E^2}\Big| \equiv \Delta t \tag{6.11}$$

upon the substition $t_2 \to L_0$ which defines the distance source-detector. Note that we could just as well perform $t_1 \to L_0$ and obtain the same result. Eq. (6.11) is generalized to

$$\Delta t_{ij} = \Big|\frac{\Delta m^2_{ij} L_0}{2E^2}\Big| \tag{6.12}$$

for the three-flavor scenario. The physical interpretation of Eq. (6.12) is that if the mass eigenstate $|\nu_j\rangle$ arrives within a time interval Δt_{ij} after the mass eigenstate $|\nu_i\rangle$, coherent oscillations can be detected even though the eigenstates are spatially separated. Δt_{ij} is then the coherence time interval associated with detection of neutrinos. The magnitude of the interval clearly depends on several parameters, and will be estimated for solar neutrinos in the following section.

6.2.2 Solar neutrinos

Consider the sun as a neutrino factory. Neutrinos produced in the sun are emitted with a wide variety of energies, thus also leading to different energy spreads for the wave packets dependent on which line the neutrino originated from, i.e. from *pp* line, ^{8}B line, *pep* line et.c. We shall consider the common ^{7}Be line. Now, the energy spread for the outgoing neutrinos is related to factors such as Doppler shifts and collisions of the emitting atoms. The author of Ref. [28] points out the small size of the captured electron wave packets as the largest contribution to incoherence. The argument in its essence is that the electron and neutrino wave packet sizes, denoted as d_e and d_{ν_e}, are related by

$$\frac{d_{\nu_e}}{c} = \frac{d_e}{v_e}, \tag{6.13}$$

where v_e is the velocity of the electron. The thermal energy of electrons at the sun's core where $T \sim 15 \times 10^6$ K corresponds to a velocity of $v_e = 0.087c$. Estimating the extension of the electron wave packet to be of the same order of magnitude as the thermal wave length $\Lambda = 2\pi/\sqrt{3m_e kT}$, one arrives at the energy spread $\Delta E = (2\pi v_e/\Lambda) = 2.06$ keV. The largest flux for the ^{7}Be line is achieved for 0.87 MeV neutrinos (see Ref. [30]) which enables us to write down all essential parameters for this case in Tab. 6.1. Inserting these values into Eq.

Table 6.1: Considering the sun as neutrino factory. Essential parameters for the ^{7}Be line.

Parameter	Value
Kinetic energy E	0.86 MeV
Energy spread ΔE	2.06 keV
Distance source-detector L_0	1 AU $= 1.49 \times 10^{11}$ m
Square mass difference Δm^2	7.1×10^{-5} eV^2

(6.7) produces $L^{\text{SOL}}_{\text{coh},c} = 1.25 \times 10^7$ m, where c denotes this particular source of incoherence, anticipating that there could be others. Since $L_0 \sim 10^{11}$ m for solar neutrinos, this result implies that they should be incoherent when arriving at Earth.

The observant reader will notice that this source of incoherence really is a consequence of a fundamental axiom in the theory of quantum mechanics itself, namely the uncertainty principle of Heisenberg, $\Delta x \Delta p \sim 1/2$. Denoting this coherence length $L^{\text{SOL}}_{\text{coh},c}$ as before, it follows that this quantity must obey

$$L^{\text{SOL}}_{\text{coh},c} \sim \frac{8E^2\pi\Delta x}{\Delta m^2_{\text{SOL}}}, \tag{6.14}$$

which is exactly what we have used in the above analysis. Other sources of incoherence are of no interest here, since the only relevant coherence length in a given scenario clearly is $L_{\text{coh}}^{\text{SOL}} \equiv \min\{L_{\text{coh},i}^{\text{SOL}}\}$. As a result, neutrinos emanating from the sun cannot be assumed to be coherent since $L_{\text{coh}}^{\text{SOL}} \ll L_0$. If the neutrinos are no longer coherent upon arrival at Earth, the oscillation probability is reduced to the classical expression of Eq. (6.5) and all phase information is lost.

But due to our argument in the end of Sec. 6.2, the possibility of detecting oscillations can still not be completely excluded. We saw that if the neutrino mass eigenstates arrive at the detector within the coherence time interval of the detection process, an interference pattern, i.e. oscillation, could still be registred even though the mass eigenstates no longer spatially overlap. The coherence time interval is directly correlated to the precision ε to which one can determine the kinetic energy E of the neutrino interacting with the detector. For our ^{7}Be line, Eq. (6.12) dictates that our detector must have an accuracy of $\varepsilon < 7.26 \times 10^{-13}$ eV. Such a detector precision is not possible, so the solar neutrino flux must be considered as incoherent.

It is important to note that even though the solar neutrinos certainly are incoherent upon arrival at Earth, oscillations can *still* be indirectly detected through matter effects. As the neutrinos traverse through several media on their way from the sun, the effective oscillation probability must be averaged out for each medium with its corresponding mixing angle θ_m. One can understand this by considering the day-night effect of solar neutrinos which in short states that there is an asymmetry in the solar neutrino flux between day- and night measurements. This is due to the fact that the neutrinos will pass through Earth, experiencing matter effects, during night, whereas the neutrinos hit the detector directly during the day. For a discussion of this in the three-flavor case, consider for instance Ref. [31].

6.2.3 Atmospheric neutrinos

Atmospheric neutrinos have their origin in cosmic rays colliding with nuclei in Earth's upper atmosphere and thus creating pions. The pions decay to $\pi^+ \to \mu^+ + \nu_\mu$ and $\pi^- \to \mu^- + \overline{\nu}_\mu$, while the muons disintegrate further to $\mu^+ \to e^+ + \overline{\nu}_\mu + \nu_e$ and $\mu^- \to e^- + \nu_\mu + \overline{\nu}_e$. Atmospheric neutrinos are in general much more energetic than their solar relatives, reaching energies as high as several GeV. This means that $\nu_\mu \to \nu_\tau$ are allowed and dominating the atmospheric neutrino scenario. In fact, the observations of high-energy ν_e yield results that are statistically consistent with zero oscillations to this flavor. The best-fit values are $\Delta m^2_{\text{ATM}} = 2.5 \times 10^{-3}$ eV^2 and $\theta^{\text{ATM}} = 0.78$ (see Tab. 3.1).

In order to say something about the coherence length for atmospheric neutrinos, we first identify the pion finite lifetime as a possible source of incoherence. Ref. [29] suggests that the corresponding energy spread due to this effect is given as $\Delta E_a = \Gamma_{\pi^+}/\pi$, where Γ_{π^+} is the decay halfwidth of the pion. This gives

$$L_{\text{coh},a}^{\text{ATM}} = \frac{4E^2}{\Gamma_{\pi^+} \Delta m^2_{\text{ATM}}}, \tag{6.15}$$

leading to $L_{\text{coh},a}^{\text{ATM}} = 1.39 \times 10^{19}$ m when assuming an $E = 10$ GeV atmospheric neutrino, since the halfwidth is $\Gamma_{\pi^+} = 1/(3.44 \times 10^{12})$ s^{-1} (see Particle Data Group [11]). This coherence length is $\mathcal{O}(10^4)$ l.y., and can therefore be neglected. For consistency, we should also calculate

the contribution from the finiteness of the muon lifetime. With $\Gamma_{\mu^+} = 3 \times 10^{-16}$ MeV (see Particle Data Group [11]), one obtains the coherence length

$$L^{\text{ATM}}_{\text{coh},b} = \frac{4E^2}{\Gamma_{\mu^+}\Delta m^2_{\text{ATM}}} = 1.32 \times 10^{-7} L^{\text{ATM}}_{\text{coh},a}. \tag{6.16}$$

Although seven orders of magnitude smaller than the coherence length due to the unstable π^+, this coherence length is of no physical significance.

The incoherence as a consequence of quantum mechanical uncertainty reads $L^{\text{ATM}}_{\text{coh},c} \sim 8E^2\pi\Delta x/\Delta m^2$, just as in the previous section. To obtain the magnitude, we need to estimate the spatial width Δx of the neutrino wave packet. There is no obvious way of doing this, but we can at least put a coherence restriction on the spatial width if we are to observe any oscillations, namely $L^{\text{ATM}}_{\text{coh},c} > 20$ km. This translates directly to $\Delta x > 1.99 \times 10^{-20}$ m for our 10 GeV neutrino. Is this a reasonable number? Well, comparison to the solar neutrino width of $\mathcal{O}(10^{-6})$ cm indicates that it shouldn't be too far-fetched, but we are really just performing an educated guess.

6.2.4 Accelerator neutrinos

In the accelerator neutrino scenario, high energy protons with energies of $\mathcal{O}(\text{GeV})$ collide with a metal target to produce μ^+ which decay further to $\mu^+ \to e^+ + \nu_e + \overline{\nu}_\mu \overset{\text{Oscillations}}{\longrightarrow} \overline{\nu}_e + p \to n + e^+$. This decay chain is indirectly observed by registring the energy spectrum of the positron [6]. Information is acquired concerning neutrino mixing parameters by looking for CC reactions with $\overline{\nu}_e$ in a beam originally consisting of $\overline{\nu}_\mu$. Typical parameters for short- and long-baseline accelerator experiments are shown in Tab. 6.2.

There is a conflict between the coherence length and oscillation term $\mathcal{W} = \sin^2(L\Delta m^2/4E)$ with respect to the distance L_0 where one should place the detector. The detector must be placed within the distance of the coherence length for oscillations to be observable, but the oscillation term gets bigger the farther away from the source we place our detector. The only compromise possible is to place the detector at a distance almost equal to the coherence length L_{coh}.

Table 6.2: Essential parameters for short-baseline vs. long-baseline accelerator neutrino experiments with data from Refs. [5, 6].

Quantity	**Short-baseline**	**Long-baseline**
Baseline length L_0 (km)	10^{-1}	$10^2 - 10^3$
Neutrino energy E (GeV)	$1 - 10$	10
Δm^2 sensitivity (eV^2)	$10^{-1} - 10^{-2}$	$10^{-2} - 10^{-3}$

Short-baseline accelerator

To consider short-baseline accelerator neutrinos as coherent, we impose the condition that $L_{\text{coh}} > 1$ km. Eq. (6.7) provides an upper limit for the neutrino energy spread ΔE for fixed E and Δm^2. In the case of CPT-invariance, it is necessary to use the global best-fit $\Delta m^2_{\text{SOL}} = 7.1 \times 10^{-5}$ eV^2 for $\overline{\nu}_\mu \to \overline{\nu}_e$ oscillations, while the LSND results from Ref. [20]) call

for $\Delta m^2_{\rm LSND} = 1.2\ {\rm eV}^2$. Fig. 6.3 contains a plot of the ratio $\Delta E/E$ that satisfies the coherence condition for both choices of the square mass difference.

Long-baseline accelerator
Consulting Tab. 6.2, we impose the condition $L_{\rm coh} > 1000$ km in order to consider long-baseline accelerators as coherent. The resulting ratio $\Delta E/E$ is illustrated in Fig. 6.3.

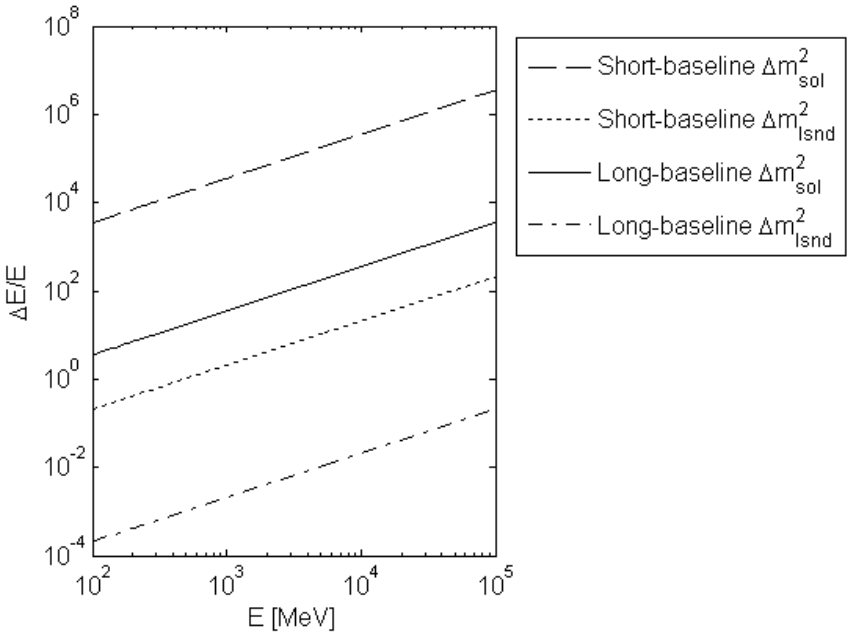


Figure 6.3: Upper limits for $\Delta E/E$ in the short- and long-baseline accelerator neutrino case, using $\Delta m^2_{\rm SOL}$ and $\Delta m^2_{\rm LSND}$.

Accordingly, both types of accelerator neutrinos can be considered coherent for solar best-fit parameters even for energy spreads as large as $\Delta E \sim E$. LSND parameters would introduce stricter limits on ΔE to justify coherence.

6.2.5 Reactor neutrinos

Reactor experiments display neutrino energies of $\mathcal{O}$(MeV), while the baseline length L_0 is subject to a large variation. L_0 ranges from 1 km for the CHOOZ experiment to $\simeq 200$ km for the KamLAND detector site (see *e.g.* Ref. [18]). Nuclear reactors give rise to a flux of $\overline{\nu}_e$ as a biproduct of neutron decay. Oscillations are then indirectly observed through an abscence of $\overline{\nu}_e$ in the neutrino beam after a distance L, due to the process $\overline{\nu}_e \to \overline{\nu}_\mu$. Now, the required coherence length for a neutrino detection experiment is dependent on the baseline length, since we want $L_{\rm coh} > L_0$. Fig. 6.4 plots the corresponding upper limits on $\Delta E/E$ for several baseline lengths, using solar best-fit parameters.

Naturally, the restriction on ΔE becomes stricter for increasing $L_{\rm coh}$. In the following, we shall assume that the energy spread is such that both accelerator and reactor neutrinos can

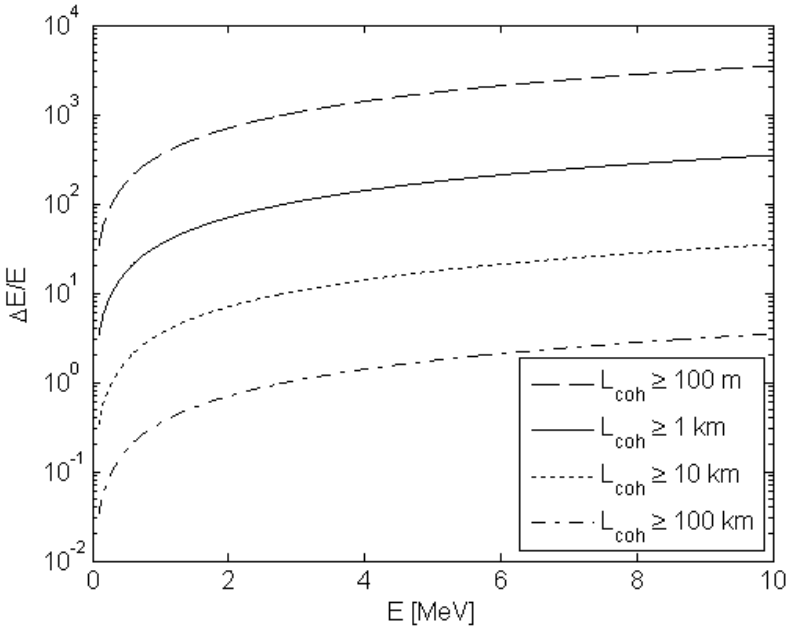


Figure 6.4: Upper limits for $\Delta E/E$ for reactor neutrinos with varying baseline, using Δm^2_{SOL}.

be considered coherent.

6.3 Restrictions on mixing parameters

In this section, we consider the restrictions placed on the neutrino mixing parameters $\{\Delta m^2, \theta\}$ by exploiting a single non-adiabatic density shift. Right from the start, we can exclude the solar and atmospheric neutrino species. As we have seen, there are problems associated with considering solar neutrinos as coherent. Thus, we cannot say anything useful about the phase information at a given point in spacetime, corresponding to the averaging of oscillation probability described in Eq. (6.5). As far as atmospheric neutrinos are concerned, we need a non-zero concentration of either muons or tauons to see any change in oscillation pattern from the vacuum case, as described in Sec. 5.1.1. Since Earth is short on both types of particles, there is no way we can exploit our idea to study the deviation $\Delta P_{\mu\tau}$. This leaves us with accelerator and reactor neutrinos.

6.3.1 Accelerator neutrinos

Restricting ourselves to realistic detector dimensions, consider an experimental setup as shown in Fig. 6.5a).

We have assumed that the distance source-detector L_0 is sufficiently small to operate with coherent neutrinos intruding the medium, which should not be a problem according to our analysis in Sec. 6.2. This particular experimental setup is beneficial, since we are looking for a medium with as high density as possible (to make $\Delta\theta$ as large as possible), and as large d as possible (so that the oscillation probability will increase significantely from zero). Assuming

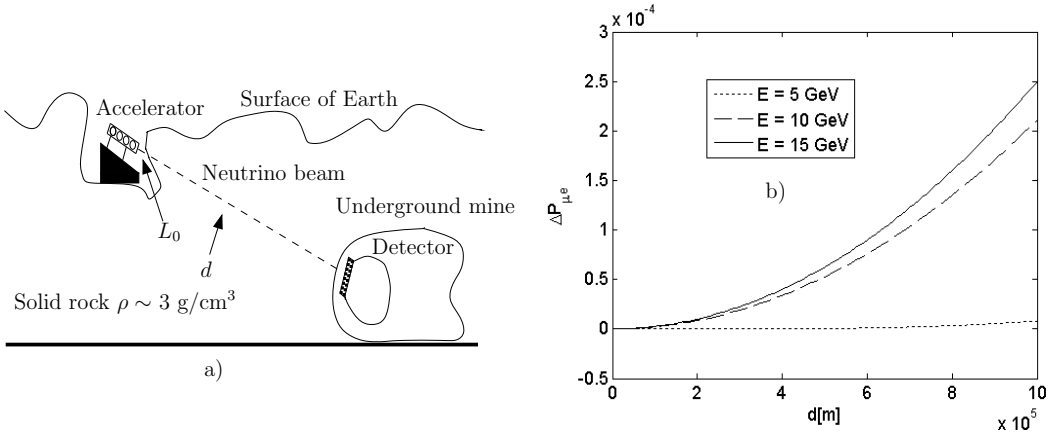


Figure 6.5: a) Hypothetical long-baseline accelerator neutrino scenario. b) $\Delta P_{\mu e}$ for $\overline{\nu}_\mu \to \overline{\nu}_e$ oscillations, using solar best-fit parameters. $L_0 = 100$ m, and material density corresponding to solid rock, $\rho \simeq 3$ g/cm^3, have been used.

solid rock of density $\rho \sim 3$ g/cm^3, the deviation $\Delta P_{e\mu}$ is illustrated in Fig. 6.5b). It is true that there most certainly are local variations in the rock density, but these are assumed to vary in an adiabatic manner, such that the corrections are very small.

As is seen from the graph, a deviation of $\mathcal{O}(10^{-4})$ can be expected at distances of several hundred kilometers. Such a small deviation would drown in statistical uncertainties from the detector precision. We therefore conclude that no realistic accelerator neutrino detection experiment could take advantage of the implications of a non-adiabatic density shift in the trajectory of the neutrino beam.

6.3.2 Reactor neutrinos

Similar to the accelerator neutrino scenario, we propose a detection setup where the neutrino beam traverses through rock before hitting the detector, as shown in Fig 6.6. The setup in b) offers the advantage of adjusting the parameters L_0 and d by simply moving the cars, thus obtaining a larger set of data values. A plot of the deviation between vacuum and MSW-adjusted oscillation probability $\Delta P_{e\mu}$ is shown in Fig. 6.6c).

Similar to accelerator neutrinos, the deviation is of $\mathcal{O}(10^{-4})$ for maximal distances of several hundred kilometers. Again, the difference is too small to produce any statistically significant restrictions.

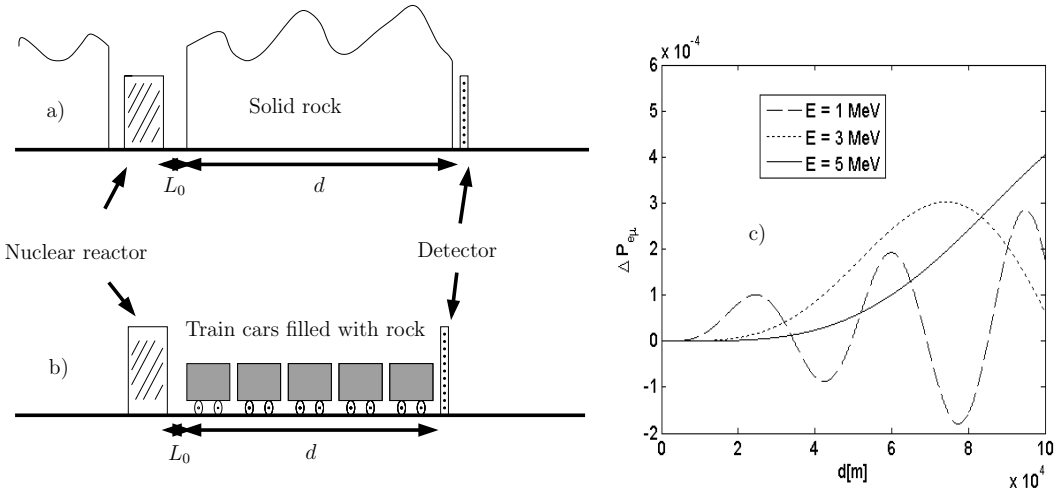


Figure 6.6: Idea for exploiting the MSW-effect for reactor neutrinos using a) natural structures on Earth as medium, and b) train cars filled with a substance (for instance rock). c) Deviation $\Delta P_{e\mu}$ for reactor neutrinos. $L_0 = 100$ m, and material density corresponding to solid rock, $\rho \simeq 3$ g/cm^3, has been used.

Chapter 7

Concluding remarks

The main result of this thesis is the analytical treatment of neutrino oscillations in the presence of a single and multiple step-wise density shifts. Having laid the foundation of neutrino interactions and oscillations in the early chapters, we then showed that it is possible to find a set of resonance parameters in the case of multiple density shifts that leads to a complete flavor conversion for both neutrinos and antineutrinos, regardless of the source (see Sec. 5.3). Confining ourselves to realistic detection setups, however, it is not possible to achieve the exact values for the resonance parameter set.

Pursuing the idea with a single unit-step density shift, results were displayed for different neutrino sources (see Sec. 6.3). When taking coherence arguments and matter effects into account, only reactor and accelerator neutrinos were found to be fit subjects for manipulation. Unfortunately, the resulting oscillation probability in matter cannot be significantely altered for realistic detector dimensions, only deviating about 0.1% from the vacuum oscillation probability.

As an appetizer and inspiration for further research of neutrino interactions with matter, consider the neutrino as an energy source substitute for the dominant fossile fuel industry. Neutrinos pervade both space outside and within Earth's atmosphere, carrying with them great amounts of kinetic energy. Great is also a fitting word to describe the potential of neutrinos as a future energy source, given that we find ways to make them interact much more frequently than we are able to do today. Imagine for instance space shuttles being powered by a practically endless supply of energy from solar neutrinos roaming our interplantetary space.

To make this more quantitative, consider a constant neutrino flux of $\sim 10^{11}$ cm^{-2} MeV^{-1} at the surface of Earth for neutrinos with $E \in [0, 0.5]$ MeV (see *e.g.* Ref. [30]). This is readily converted into an effect of 40 W/m^2, which can be compared to the solar constant (the amount of incoming solar radiation per unit area at the surface of Earth) of roughly 1367 W/m^2. In other words, the neutrino kinetic energy constitutes about 3% of the solar radiation. However, the neutrinos are available during the night as well, and we have not considered the contribution from atmospheric neutrinos.

Before getting too carried away, it is clear that we are very far from implementing such an

energy source as of today. But small steps are constantly taken towards a fuller understanding of neutrino interactions and how one might be able to manipulate these interactions to our benefit. Who knows what the future will bring?

Bibliography

[1] F. Reines, C. L. Cowan, F. B. Harrison, A. D. McGuire, H. W. Kruse, *Phys. Rev.* **117**, (1960)

[2] R. Davis, *Prog. Part. Nucl. Phys.*, Volume 32, p.13-32 (1994)

[3] Y. Fukuda *et al.*, (The Kamiokande collaboration), *Phys. Rev. Lett* **77**, 1683 (1996).

[4] B. Pontecorvo, *Sov. Phys. JETP 7*, 172 (1958).

[5] M. C. Gonzalez-Garcia, Yosef Nir, *Rev. Mod. Phys.* **75**, p.345-402 (2003).

[6] T. K. Kuo, J. Pantaleone, *Rev. Mod. Phys* **61**, p.941-958 (1989).

[7] A. Gouvêa, C. Peña-Garay *Phys. Rev.* D **64**, 113011 (2001).

[8] Q. R. Ahmad *et. al* (SNO collaboration), *Rev. Mod. Lett* **87**, 071301 (2001).

[9] J. E. Kim, P. Langacker, M. Levine, H. H. Williams, *Rev. Mod. Phys.* **53**, p. 211-252 (1981).

[10] F. Mandl, G. Shaw, *Quantum Field Theory* (J. Wiley & Sons, Inc., 1984).

[11] S. Eidelman *et al.*, *Phys. Lett.* B **592**, 1 (2004).
Also available at `http://pdg.lbl.gov`, Particle Data Group (2005).

[12] J. Erler, *Phys. Rev.* D **63**, 071301 (2001).

[13] C. Quigg, *Gauge theories of the strong, weak, and electromagnetic interactions*, (Westview Press 1983, 1997).

[14] M. Peskin, D. V. Schroeder, *An introduction to Quantum Field Theory* (Westview Press, 1995).

[15] P. Vogel, A. Piepke, *Electron, muon, and tau neutrinos*,
`http://pdg.lbl.gov/2002/emutauneutrinos_s802.pdf`, Particle Data Group (2001).

[16] M. Tegmark *et al.*, *Phys. Rev.* D **69**, 103501 (2004).

[17] M. Jacobson, T. Ohlsson *Phys. Rev.* D **69**, 013003 (2004).

[18] C. Bemporad, G. Gratta, P. Vogel, *Rev. Mod. Phys.* 74, 297-328 (2002).

[19] F. Boehm, P. Vogel, *The Physics of Massive Neutrinos* (Cambridge Univ. Press, Cambridge, 1987).

[20] C. Athanassopoulos *et. al*, *Phys. Rev. Lett.* 81, 1774-1777 (1998).

[21] Fermi National Accelerator Laboratory, `http://www-boone.fnal.gov/`, (2005).

[22] L. Wolfenstein, *Phys. Rev.* D **17**, 2369-2374 (1978).

[23] J. F. Beacom, W. M. Farr, P. Vogel, *Phys. Rev.* D **66**, 033001 (2002).

[24] W. C. Kim, A. Pevsner, 1993, *Neutrinos in Physics and Astrophysics*, Contemporary Concepts in Physics, No. 8 (Harwood Academic, Chur, Switzerland) (1993).

[25] E. K. Akhmedov, *Nucl. Phys.* B **538** p. 25-51 (1999).

[26] E. K. Akhmedov, A. Y. Smirnov, *Phys. Rev. Lett.* **85** p. 3978 (2000).

[27] MatWeb, `http://www.matweb.com`, Material Property Data (2005).

[28] K. Kiers, S. Nussinov, N. Weiss, hep-ph/9506271 (1995)

[29] W. Grimus, P. Stockinger, S. Mohanty *Phys. Rev.* D **59**, 013011 (1999).

[30] J. N. Bahcall, A. M. Serenelli, S. Basu, astro-ph/0412440v3 (2005)

[31] M. Blennow, T. Ohlsson, H. Snellman, *Phys. Rev.* D **69**, 073006 (2004).